

1 **Bias correction of modelled urban temperatures with**
2 **crowd-sourced weather data**

3 **O. Brousse¹, C. Simpson¹, O. Kenway², A. Martilli³, E. S. Krayenhoff⁴, A.**
4 **Zonato⁵, C. Heaviside¹**

5 ¹Institute of Environmental Design and Engineering, University College London

6 ²Centre for Advanced Research Computing, University College London

7 ³Center for Energy, Environment and Technology (CIEMAT)

8 ⁴Department of Civil, Environmental and Mechanical Engineering, University of Trento

9 ⁵School of Environmental Sciences, University of Guelph

10 **Key Points:**

- 11 • Spatially heterogeneous urban climate simulation biases exist
12 • Bias-correction using crowd-sourced weather data can be applied
13 • The bias-correction is necessary prior to urban climate impact studies

Corresponding author: Oscar Brousse, o.brousse@ucl.ac.uk

14 **Abstract**

15 Urban climate model evaluation often remains limited by a lack of trusted urban weather
16 observations. The increasing density of personal weather stations (PWS) make them a
17 potential rich source of data for urban climate studies that address the lack of representative
18 urban weather observations. In our study, we demonstrate that PWS data not only improve
19 urban climate models' evaluation, but can also serve for bias-correcting their output prior
20 to any urban climate impact studies.

21 After simulating near-surface air temperatures over London and south-east England
22 during the hot summer of 2018 with the Weather Research Forecast (WRF) model and
23 its Building Effect Parameterization with the Building Energy Model (BEP-BEM) acti-
24 vated, we evaluated the modelled temperatures against 407 urban PWS and showcased a
25 heterogeneous spatial distribution of the model's cool bias that was not captured using of-
26 ficial weather stations only. This finding indicated a need for spatially-explicit urban bias
27 corrections of air temperatures, which we performed using an innovative method using ma-
28 chine learning to predict the models' biases in each urban grid cell. Our technique is the
29 first to consider that urban temperatures are heterogeneously accurate in space and that
30 this accuracy is not linearly correlated to the urban fraction. Our results showed that the
31 bias-correction was beneficial to bias-correct daily-minimum, -mean, and -maximum tem-
32 peratures in the cities.

33 We recommend that urban climate modellers further investigate the use of PWS for
34 model evaluation and derive a framework for bias-correction of urban climate simulations
35 that can serve urban climate impact studies.

36 **Plain Language Summary**

37 Urban climate simulations are subject to spatially heterogeneous biases in urban air
38 temperatures. Common validation methods using official weather stations do not suffice for
39 detecting these biases. Using a dense set of personal weather stations in London, we detect
40 these biases before proposing an innovative way for correcting them with machine learning
41 techniques. We argue that any urban climate impact study should use such technique if
42 possible and that urban climate scientists should continue investigating paths to improve
43 our methods.

44 **1 Introduction**

45 Although decades following the 1960s have seen an increase in the body of literature
46 on urban climates (Oke et al., 2017), the scales of applicability and the transferability of
47 their outcomes are often limited. This can partially be attributed to the lack of observations
48 representative of the variety of existing urban climates in cities. To address this impedi-
49 ment, two major solutions were proposed over the past 20 years: firstly, the development
50 of urban surface energy balance and climate models (e.g., Masson (2000), Martilli et al.
51 (2002), Wouters et al. (2016)) that are coupled to regional climate models, and secondly,
52 the increased interest towards crowd-sourced and low-cost weather sensors (e.g., Muller et
53 al. (2015), Chapman et al. (2017), Fenner et al. (2017), Meier et al. (2017)). Indeed, after
54 proper validation and parameterization, urbanized regional climate models, with their ur-
55 ban climate models (UCMs) activated, offer an unprecedented opportunity to represent the
56 impact of cities on a wide variety of weather variables at very high spatial and temporal
57 resolutions – an opportunity further supported by the recent development of global stan-
58 dardized land use land cover datasets designed for urban climate studies that permit their
59 parameterization in cities formerly deprived of these data (see the World Urban Dataset
60 and Access Portal Tool (WUDAPT) project; Ching et al. (2018), Demuzere et al. (2022)).
61 Likewise, after proper filtering and quality control (Napoly et al., 2018; Fenner et al., 2021),

62 crowd-sourced personal weather sensors (PWS) permit the extension of sensing networks
63 into urban environments that were formerly not studied despite the fact that PWS often
64 do not meet the standards imposed by official meteorological offices for implementation of
65 weather stations.

66 Nonetheless, both these tools have limitations. For instance, PWS observations are
67 of lower reliability and accuracy than official weather stations and cover only recent years,
68 booming after 2015 (Brousse et al., 2022). Relating the observed weather to the underlying
69 environmental characteristics can also be difficult, as requirements for the site description
70 are modest to non-existent. Recent efforts have however managed to bridge this information
71 gap by using earth observations, and in particular the universal standardized Local Climate
72 Zones land-use land-cover classification (Stewart & Oke, 2012) which permitted not only
73 the study of key weather variables in cities, like near-surface air temperature (e.g., Fenner
74 et al. (2019), Potgieter et al. (2021), Benjamin et al. (2021), Varentsov et al. (2021)),
75 but also their prediction via machine learning (Venter et al., 2020, 2021). Though these
76 mapping efforts, aided by the development of machine learning algorithms, are substantial
77 achievements, better predictions were usually achieved at low temporal resolution (e.g.,
78 weekly or seasonally), thus calling for more research to be done in order to reach improved
79 performance at daily or hourly time-steps. This research could help comparing the outputs of
80 physical models, like UCMs, to predicted maps of urban-specific weather variables obtained
81 via PWS.

82 Indeed, UCMs are computationally expensive, require complex and energy-consuming
83 computational infrastructures, and require prior expert-knowledge to be properly used. For
84 example, depending on the study in terms of city-location, domain dimension, horizontal
85 and temporal scales, or meteorological variables of interest, users need to ascertain that their
86 models are meaningfully parameterized with the right physical and dynamical schemes, and
87 forced by representative initial and boundary atmospheric conditions. These requirements
88 are usually verified through sensitivity tests performed before running real-case scenarios,
89 where model outputs are compared against weather measurements obtained from official
90 weather stations. Then, users balance the need for accuracy with computational limitations.
91 Notwithstanding, hazardous uncertainties exist even after sensitivity studies are performed,
92 as shown by Bassett et al. (2020) who demonstrated that the starting time of the simu-
93 lation had a noticeable impact on the modelled air temperature at 2 m in London during
94 the summer 2018. Moreover, because of the lack of official weather stations in cities, mea-
95 suring existing uncertainties per urban climate archetype is not feasible. This means that
96 certain urban environments are poorly evaluated and hence modelled, assuming that UCMs
97 will perform similarly under all constraints imposed by the variety of urban environments
98 that compose a city. In face of this challenge, quality-checked crowd-sourced PWS allow
99 monitoring for a range of urban environments. They can therefore serve the evaluation of
100 UCMs, as Hammerberg et al. (2018) demonstrated over Vienna. But the potential of PWS
101 may even be greater, particularly when used jointly with or in parallel to UCMs. In fact,
102 a recent study by Sgoff et al. (2022) improved the weather forecasting of the Icosahedral
103 Nonhydrostatic Model (ICON; Zängl et al. (2015)) at a horizontal resolution of 2 km over
104 Germany by assimilating the data provided by PWS for air temperature and relative humid-
105 ity at 2 m height. Although data assimilation is done while UCMs are running, PWS could
106 also be used to subsequently bias-correct urban climate simulations. To date, no study has
107 explored how PWS could be used to bias-correct simulated urban climates despite the need
108 for realistic urban weather data of present and future urban climates to perform impact
109 studies that can guide decision-making.

110 Oleson et al. (2018) already noted the need of a global dataset on urban weather
111 observations to properly bias-correct simulated urban climates: we here propose to use
112 the densifying network of PWS to bias-correct urban climate simulations for urban climate
113 impact studies. Common practice in bias-correction of urban climate simulations is to apply
114 a single correction by the mean bias at official weather stations' rural sites, thereby assuming

115 that the urban heat island phenomenon is accurately represented by the UCM (e.g., Lauwaet
116 et al. (2015), or Oleson et al. (2018)). Some studies however tried considering the urban effect
117 by linearly transforming the bias-correction coefficient via an urbanization ratio calculated
118 at each grid cell, like in Wouters et al. (2017) over Belgium. Assuming that urban climate
119 simulations biases cannot be linearly related to the urban fraction only, we decided to test
120 whether urban in-situ observations can be used to perform an urban-specific bias-correction
121 of air temperatures driven by machine learning. We hereby hypothesize that such innovative
122 bias-correction method would be beneficial for urban heat impact studies by improving the
123 UCM outputs on which they rely. Such innovations are needed to better assess the heat
124 burden in cities (Nazarian et al., 2022).

125 To respond to these questions through the scope of urban near-surface temperatures,
126 we: i) evaluated the ability of the complex three-dimensional UCM embedded in WRF
127 – the Building Effect Parameterization coupled with its Building Energy Model (BEP-
128 BEM) – to accurately represent the urban impact on air temperatures under two boundary
129 layer schemes for the summer 2018 in south-east England using official weather stations
130 and PWS separately to show their added value for detecting spatially heterogeneous urban
131 temperature biases; ii) used machine learning regressions to predict the models’ daily air
132 temperature biases in the urban environment and bias-correct the two simulations suggested
133 in part i – which allowed us to determine an optimal time-step at which the bias-correction
134 should be performed to optimize the outputs.; and iii) compared the two bias-corrected
135 products against the predicted daily air temperatures using only PWS measurements to
136 investigate how realistic the bias-corrected products are. In parallel, to illustrate the benefit
137 gained from the bias-correction for impact studies, we showcase how the bias-correction
138 leads to different population weighted temperatures in the Greater London area.

139 It is important to consider that our study does not try to estimate how a bias-corrected
140 modelled product is better compared to a predicted product from observations for urban
141 climate impact studies. We hereby simply try to demonstrate that any urban climate
142 impact work that is based on urban climate modelling should pursue a spatially explicit
143 bias-correction specific to urban areas.

144 2 Methods

145 2.1 Model setup and region of interest

146 We focused our study on the south-eastern parts of England, centred over the metropolis
147 of London, host to approximately 9 million inhabitants. We chose to model the impact of
148 urbanization on 2 m air temperature in London during the Summer of 2018, since it was
149 one of the hottest summers in recent years. Indeed, the British Isles heatwaves of summer
150 2018 is considered to be the hottest summer on record for mean temperature (McCarthy et
151 al., 2019), with maximum daily temperatures often over-passing 30 °C (Figure 2). Record
152 temperatures, recently over-passed during the 2019 and 2022 summers, were recorded on
153 the 26th of July with a maximum of 34.4 °C measured at London’s Heathrow airport.

154 To model the impact of the urban areas of London and south-east England on local
155 meteorology, we used the Weather Research Forecast (WRF) regional climate model version
156 4.3 and activate the embedded Building Effect Parameterization (BEP; Martilli et al. (2002))
157 urban climate model with its partner Building Energy Model (BEM; Salamanca et al. (2010);
158 Salamanca and Martilli (2010)) – hereafter referred to as BEP-BEM. We ran the model at
159 a horizontal resolution of 1 x 1 km following a two-way nesting strategy where the outer
160 domain is forced by ERA5 6-hourly data at 25 km with 199 by 199 grid points and the two
161 intermediate domains are run at horizontal resolutions of 9 and 3 kilometres with 252 by
162 241 and 210 by 180 grid points, respectively (Figure 2, upper panel). Initial land surface
163 conditions were provided by the default MODIS 5-arc-second land use dataset provided by
164 the WRF community while sea surface temperatures were updated 6-hourly out of ERA-5.

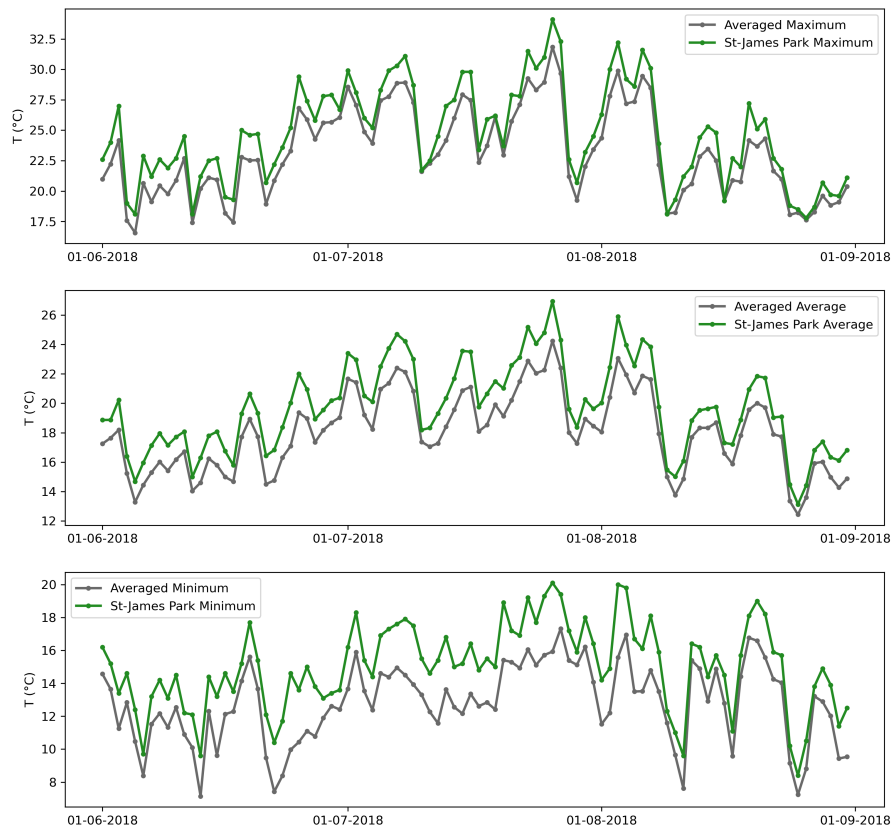


Figure 1. Daily minimum, average and maximum temperatures observed by the Met Office MIDAS automatic weather stations. The urban St-James' Park station in central London (green) is always hotter than the average temperature of all MIDAS stations in south-east England (grey)

165 We ran the model in parallel over 200 CPUs using restarts every four days of simulation.
 166 We started the simulations on the 25th of May 2018 and end them on the 31st of August
 167 2018, considering the first 7 days of simulation as spin-up time.

168 All domains used the same physical and dynamical parameterizations which we obtained
 169 out of preliminary testing done over the two hottest days of the summer 2018 – 26th and
 170 27th of July 2018 (see Supplements S1). We thereby used the WRF Single-moment 3-
 171 class microphysics scheme (Hong et al., 2004), the Dudhia shortwave and RRTM longwave
 172 schemes (Dudhia, 1989; Mlawer et al., 1997), and the revised MM5 surface layer scheme
 173 (Jiménez et al., 2012). In the first domain, the Kain–Fritsch convection scheme was activated
 174 (Kain, 2004) and then turned off in the second and third domains, which were at convection-
 175 permitting scales. We set the model top at 50 hPa with an additional 5000 m damping layer
 176 and subdivided the atmosphere into 56 vertical layers. We used the Noah-MP land surface
 177 scheme (Niu et al., 2011; Z.-L. Yang et al., 2011) in its default parameterization over 4 soil
 178 layers.

179 Urban canopy parameters required by the WRF BEP-BEM model were provided via the
 180 newly standardized WUDAPT-TO-WRF (W2W) python package developed by Demuzere
 181 et al. (2021), following the Fortran version used by Brousse et al. (2016). This allowed
 182 the transfer of spatially-explicit morphological urban canopy parameters suitable for urban
 183 climate simulations via Local Climate Zones (LCZ) maps covering the inner domain (Fig-
 184 ure 2, lower panel). We use the European LCZ map by Demuzere et al. (2019). Thermal and
 185 radiative parameters are also directly derived from the LCZ classification and follow those
 186 used by Stewart et al. (2014), who used these parameters for the city of Basel, Switzerland.
 187 Each parameter for roofs, walls and roads is related to each modal LCZ of the 1 km grid
 188 cell via the URBPARAM.LCZ.TBL (see Table 1). We decided to keep the roughness length
 189 for momentum and the lower boundary for temperatures of roofs, walls, and roads identical
 190 across each LCZ. We fixed the roughness length at 1.00E-4 m for walls and at 0.01 m for
 191 roofs and roads, respectively. For the boundary temperatures, we set it at 299 K for the
 192 roofs and the walls, respectively, and at 293 K for the road. We chose to deactivate the air
 193 conditioning in our simulation because air conditioning systems are not common in residen-
 194 tial areas across London and surrounding cities, which compose the major part of the land
 195 use land cover.

196 In this study, two potential planetary boundary layers (PBL) schemes are compared in
 197 terms of performance and need of bias correction: the commonly used Bougeault-Lacarrère
 198 scheme (BouLac; Bougeault and Lacarrere (1989)) for urban simulations that use BEP-
 199 BEM, and the recently coupled YSU scheme to BEP-BEM (Hong et al., 2006; Hong & Kim,
 200 2008; Hendricks et al., 2020). Although we found that the latter performed better over the
 201 two hottest days of summer 2018 (see Appendix A), we decided to keep a simulation with
 202 BouLac as YSU has only been applied over Dallas (Wang & Hu, 2021) whereas BouLac has
 203 been used in multiple studies already (e.g., Salamanca et al. (2011), Salamanca et al. (2012),
 204 Gutiérrez et al. (2015), Tewari et al. (2017), Mughal et al. (2019)). The Mellor-Yamada-
 205 Janjic (MYJ; Janjić (1994), Janić (2001)) scheme, also available for BEP-BEM simulations,
 206 is disregarded in this study since this PBL scheme is especially used for mountainous terrain
 207 (Zonato et al., 2022), and we are modelling the relatively flat terrain of south-east England.

208 2.2 Model evaluation

209 We evaluate the model’s performances against 35 official weather stations’ measure-
 210 ments of air temperature at 2 m obtained from the UK Met Office MIDAS network (Sunter
 211 (2021), UKMO (2021); Figure 1, lower panel). To address the issue of lack of official obser-
 212 vations amongst the urban environment, we use Netatmo PWS to complement the model
 213 evaluation (Figure 1, lower panel). Prior to the evaluation, unrealistic PWS measurements
 214 were filtered out using the Crowd-QC v1.0 R package from Grassmann et al. (2018); de-
 215 tails of the method can be found in Napoly et al. (2018) and other publications such as

Table 1. Thermal and radiative parameters per LCZ based on Stewart et al. (2014). Road parameters are considering a mixture of asphalted and concrete road pavements and grass.

	Heat capacity [$J \cdot m^{-3} \cdot K^{-1}$]			Thermal conductivity [$J \cdot m^{-1} \cdot s^{-1} \cdot K^{-1}$]			Albedo			Emissivity		
	Roof	Wall	Road	Roof	Wall	Road	Roof	Wall	Road	Roof	Wall	Road
LCZ 1	1.80E+06	1.80E+06	1.75E+06	1.25	1.09	0.77	0.13	0.25	0.15	0.91	0.90	0.95
LCZ 2	1.80E+06	2.67E+06	1.65E+06	1.25	1.50	0.73	0.18	0.20	0.16	0.91	0.90	0.95
LCZ 3	1.44E+06	2.05E+06	1.63E+06	1.00	1.25	0.69	0.15	0.20	0.18	0.91	0.90	0.95
LCZ 4	1.80E+06	2.00E+06	1.54E+06	1.25	1.45	0.60	0.13	0.20	0.20	0.91	0.90	0.95
LCZ 5	1.80E+06	2.00E+06	1.50E+06	1.25	1.45	0.62	0.13	0.25	0.20	0.91	0.90	0.95
LCZ 6	1.44E+06	2.05E+06	1.47E+06	1.00	1.25	0.60	0.13	0.25	0.21	0.91	0.90	0.95
LCZ 7	2.00E+06	7.20E+05	1.38E+06	2.00	0.50	0.51	0.15	0.20	0.24	0.28	0.90	0.92
LCZ 8	1.80E+06	1.80E+06	1.80E+06	1.25	1.25	0.80	0.18	0.25	0.17	0.91	0.90	0.95
LCZ 9	1.44E+06	2.56E+06	1.37E+06	1.00	1.00	0.55	0.13	0.25	0.23	0.91	0.90	0.95
LCZ 10	2.00E+06	1.69E+06	1.49E+06	2.00	1.33	0.61	0.10	0.20	0.21	0.91	0.90	0.95

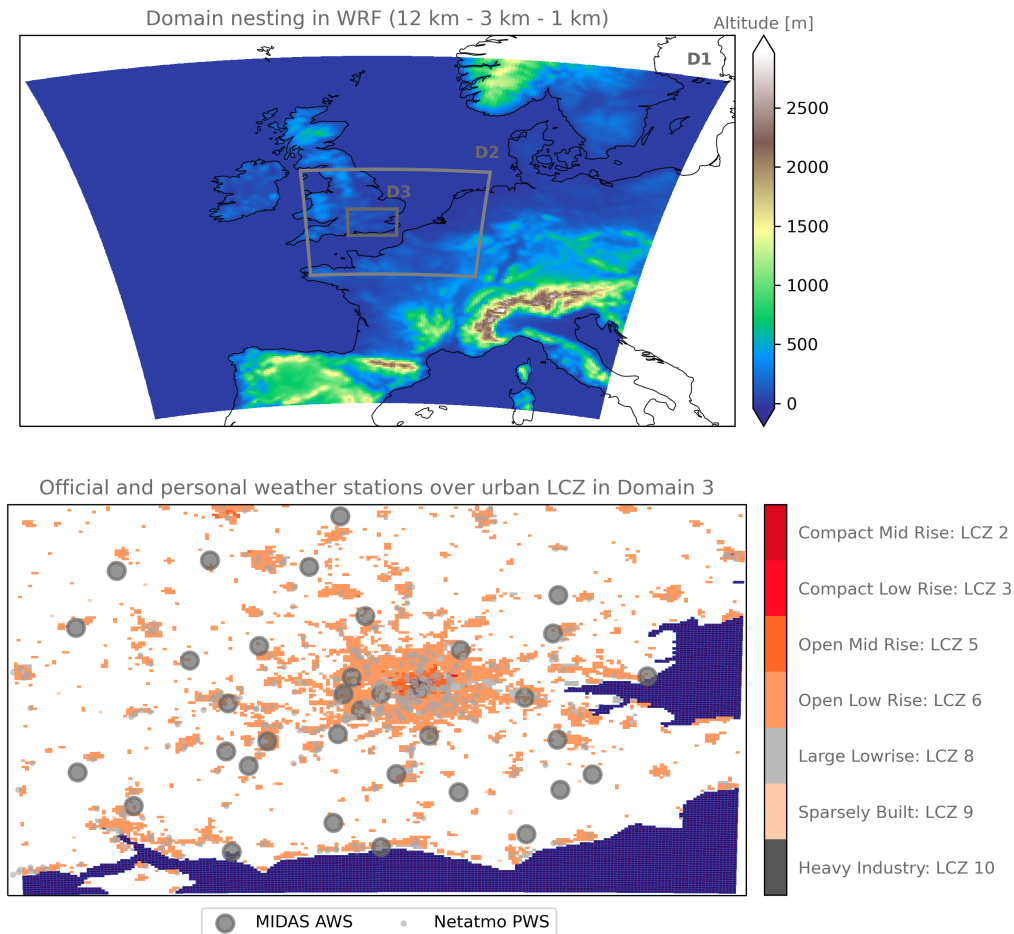


Figure 2. Domain nesting (upper) and urban land cover in the inner domain (lower). The WRF nesting strategy consists of three nested domains at 12 km (D1), 3 km (D2) and 1 km (D3) horizontal resolution. The altitude is plotted to highlight the flat terrain of south-east England covered in D3. In the lower panel, the resulting urban landcover in D3 after using the WUDAPT-TO-WRF python tool is presented in the form of Local Climate Zones (LCZ). The MIDAS official automatic weather stations (AWS) and the Netatmo personal weather stations (PWS) used for the evaluation of the model and the subsequent bias-correction using PWS only are overlaid in grey. The sea is shown in blue in the lower panel while coastlines are drawn in black in the upper panel.

216 Brousse et al. (2022), who used the same dataset over London. This resulted in 407 urban
 217 PWS suitable for evaluating the UCM. Each model simulation is evaluated using a set of
 218 common statistical indicators: the root mean squared error (RMSE), the mean absolute
 219 error (MAE), the mean bias error (MB), Spearman’s coefficient of correlation (r) and the
 220 square of Pearson’s coefficient of correlation (r^2). These metrics are obtained using the
 221 Python scikit-learn and scipy’s stats packages from Pedregosa et al. (2011) and Virtanen et
 222 al. (2020).

223 **2.3 Bias correction using personal Netatmo weather stations**

224 We expect urban climate simulations to have systematic biases that can be induced for
 225 a variety of reasons, such as: urban canopy parameters (Demuzere et al., 2017; Hammerberg
 226 et al., 2018; Zonato et al., 2020); complexity of urban climate models (Grimmond et al.,
 227 2011; Loridan & Grimmond, 2012; Lipson et al., 2021); time at which the simulation is
 228 initialised (Bassett et al., 2020); choice of initial and boundary conditions for lateral and
 229 vertical forcing (Brisson et al., 2015); or choice of model parameterizations – such as the two
 230 evaluated in this work. Hence, UCM will always present a certain degree of uncertainty that
 231 has to be coped with prior to performing urban climate impact studies that use climatic
 232 variables derived from modelled simulations to estimate the impact of the urban climate on
 233 other events (e.g. mortality, biodiversity, etc.). In our study, we decided to use machine
 234 learning regressors and benefit from the high density of PWS in south-east England to
 235 correct the air temperature biases and make the simulations usable for urban heat impact
 236 studies. To our knowledge, such technique has never proposed as a viable approach for
 237 bias-correction of urban climate simulations, probably because of the lack of observations
 238 in urban areas.

239 Indeed, the practice of bias correction is to find a transformation between modelled
 240 variables and measured variables. Common practices include adding the mean bias to the
 241 modelled variable distribution or applying a separate correction to each quantile of the
 242 distribution (Maraun & Widmann, 2018). Typically, observations are available only from
 243 official weather stations, which may not capture spatial variation within an urban area.
 244 Here, because we want to use observations which represent the spatial variation within
 245 urban areas at the 1 km scale, we developed an innovative method for bias-correction. Using
 246 regression, we predict the bias in the modelled air temperature at 2 m (T2) relative to the
 247 PWS observations at each model grid cell which has PWS observations. This prediction is
 248 based on the same set of spatially explicit morphological urban canopy parameters at 1 km
 249 horizontal resolution that were inputs to the UCM. These include the urban fraction, the
 250 surface height, the average building height, the building surface to plan area fraction (λ_b),
 251 the plan area fraction (λ_p) and the frontal area fraction (λ_f). We are therefore making the
 252 assumption that the spatial variation in the bias of the model is dependent only upon its
 253 spatial inputs.

254 We chose to bias-correct the simulated daily minimum, maximum and average T2
 255 ($T2_{min}$, $T2_{max}$, and $T2_{mean}$) using filtered PWS observations in London and south-east
 256 England. To do so, only PWS that have less than 4 hours per day without data and that
 257 are located in urban pixels with an urban fraction greater than 0 are retained – where the
 258 WRF land-use land-cover at 1 km horizontal resolution refers to an LCZ. Daily temporal
 259 scale is considered optimal as it combines a higher spatial density of measurements compared
 260 to hourly data and a lower computational requirement; it is also a commonly used temporal
 261 scale for urban heat impact studies. Daily minimum and maximum air temperatures at 2 m
 262 are defined following the Met Office Had-UK definition: minimum temperature observed
 263 from 9AM of the previous day d-1 to 9AM of the d day, and maximum temperature observed
 264 from 9AM of the d day to 9AM of the next day d+1 (Hollis et al., 2019).

265 We test the ability of 6 different regressors of increasing complexity available in the
 266 Python scikit-learn packages (Pedregosa et al., 2011) to predict the model bias based on

Table 2. Hyperparameter tuning used by each regressors

Model	Parameters Dictionary
Linear	'normalize': False
Ridge	'alpha': 1, 'normalize': True, 'random_state': 42, 'solver': 'lsqr', 'tol': 0.01
Lasso	'alpha': 1, 'normalize': False, 'random_state': 42, 'selection': 'random', 'tol': 1e-10
Random Forest	'max_features': 'sqrt', 'min_samples_leaf': 11, 'min_samples_split': 2, 'n_estimators': 400, 'random_state': 42
Gradient Boosting	'learning_rate': 0.2, 'max_depth': 3, 'max_features': 'sqrt', 'min_samples_leaf': 10, 'min_samples_split': 22, 'n_estimators': 200, 'random_state': 42, 'subsample': 0.2

267 WRF spatial urban canopy parameters only. These regressors are: dummy regression (which
 268 simply returns the mean), linear regression, Ridge regression, Lasso regression, Random For-
 269 est regression, and Gradient Boosting regression. Each of the different regressors, except
 270 the dummy regression, offers a set of parameters that can be fine-tuned to increase each
 271 regressor's performance. Hence, prior to running the daily bias-correction we use a 5 K-fold
 272 cross-validation using the Grid Search CV package from scikit-learn in Python to evaluate
 273 the impact of hyperparameter tuning on the regressors' performances based on RMSE, MAE
 274 and r^2 . The cross-validation is done over the summertime average daily mean temperature
 275 bias from the control run only, for computational reasons. We retain RMSE as the refitting
 276 score to better capture the spatial spread and extremes of T2. The resulting parameteriza-
 277 tions are given in Table2. We chose to keep the same hyperparameter tuning for all bias
 278 correction and predictions to ease comparability between the outcomes.

279 Once the hyperparameter tuning is done and prior to performing the final bias-correction,
 280 we test if the bias-correction is beneficial for palliating to the models' bias and if it also ben-
 281 efits from training the regressors at the daily time-step or if a training using the time-mean
 282 bias is sufficient. To perform this evaluation using the same metrics as in the model evalua-
 283 tion, we bootstrap each regressors 25 times, randomly sampling 80 % of the data as training
 284 and the remaining 20 % as testing – for both the daily-minimum, -maximum and -average,
 285 and their respective summer time-mean average. The average predicted daily T2_BC of
 286 all predicted T2_BC in the test sample is then compared against the observed T2 – for
 287 daily-minimum, -maximum and -average.

288 After this final step, we bias-correct both the BouLac and the YSU runs using 100 % of
 289 the PWS data to compare the spatial outcomes. We also predict T2 out of PWS' observed
 290 T2 with the same set of covariates used to predict the model bias to illustrate how divergent
 291 each bias-corrected model outputs are to a simplified predicted T2 that is not a derivative
 292 of any model constraint. Because more refined and complex techniques exist to predict
 293 air temperature from PWS and very high-resolution earth observations (e.g., Venter et
 294 al. (2020), Venter et al. (2021)), we do not evaluate these predicted temperatures which
 295 should simply be considered as an illustration of how bias-corrected products are similar or
 296 divergent to observational data.

297 Lastly, to illustrate the potential benefit of modelled air temperature bias-correction
 298 prior to urban heat impact studies, we calculate the average population weighted temper-
 299 atures – based on the United Kingdom census data from 2011 – in Greater London before
 300 and after the bias-correction.

Table 3. Average of all performance metrics calculated at each MIDAS official weather stations for hourly air temperature at 2 m for the summer period (1st June 2018 to the 31st of August 2018). Urban stations are stations located in a pixel classified as an urban LCZ in WRF and rural stations are located in other natural land-use land-cover.

	BouLac					YSU				
	RMSE	MAE	MB	r ²	r	RMSE	MAE	MB	r ²	r
All	2.33	1.82	-0.56	0.77	0.86	2.31	1.83	-0.57	0.79	0.88
Urban	2.42	1.88	-0.73	0.76	0.86	2.42	1.92	-0.93	0.77	0.87
Rural	2.32	1.81	-0.53	0.78	0.86	2.28	1.81	-0.50	0.80	0.88

3 Results

3.1 WRF simulation evaluation

When we evaluate the two model simulations against MIDAS official weather stations only, they perform similarly, demonstrating a systematic negative bias of ~ 0.55 °C on average (Table 3). The average correlation with the automatic weather stations following the squared Pearson’s r^2 is of 0.77 for BouLac and 0.79 for YSU, while using Spearman’s r it is of 0.86 and 0.88, respectively. A slight decreased performance is found in urban pixels for YSU, with an average MAE of 1.83 °C and a negative MB of 0.79 °C compared to BouLac’s 1.82 °C for MAE and -0.56 °C for MB. In general, the bias is more important at night, and, in non-urban stations, performances are similar. Hence, looking only at the models’ performances using standard in-situ observations doesn’t provide information on which model represents the urban climate more accurately.

On the other hand, comparison with PWS observations identifies differences in performance in urban areas between the models, as shown by the performance metrics plotted in Figure 3 and B1. The BouLac simulation has a stronger cool bias of -1.46 °C \pm 0.6 °C on average in the urban area, compared to YSU’s MB of -0.99 °C \pm 0.82 °C. RMSE and MAE are similar, with values of 2.79 °C \pm 0.36 °C and 2.20 °C \pm 0.32 °C for BouLac and 2.66 °C \pm 0.40 °C and 2.15 °C \pm 0.35 °C for YSU. These metrics are consistent with the MIDAS observations, highlighting a systematic cool bias of the model and a coefficient of determination (r^2) of 80 %. Importantly, the variability in the model’s performance is more greater in the YSU run – reflected by greater standard deviations of performance metrics – and, in the BouLac simulation, the metrics are more heterogeneously distributed amongst the urban area. Indeed, when we look at the YSU simulation, we can see that the model has a smaller MB in suburban areas and a greater MB in the city centre. Yet, in parallel, the correlation with the PWS is lower in the suburban areas and higher in the centre of the city. This could mean that YSU accurately represents the urban temperatures on average due to compensating effects, which we do not intend to evaluate in this study. Nevertheless, this shows how PWS are beneficial for capturing the spatial heterogeneity of each model’s performance and therefore supports the use of spatially-varying bias-correction.

3.2 Bias correction of urban climate simulations

Over our domain of study covering south-east England during the Summer 2018, both models are subject to a cold negative bias of ~ 0.5 °C on average according to official stations and of ~ 1.0 °C to ~ 1.5 °C according to PWS. But as demonstrated above, the bias of the models against PWS observations has substantial spatial variation and so the bias correction for urban heat impact studies should be spatially explicit.

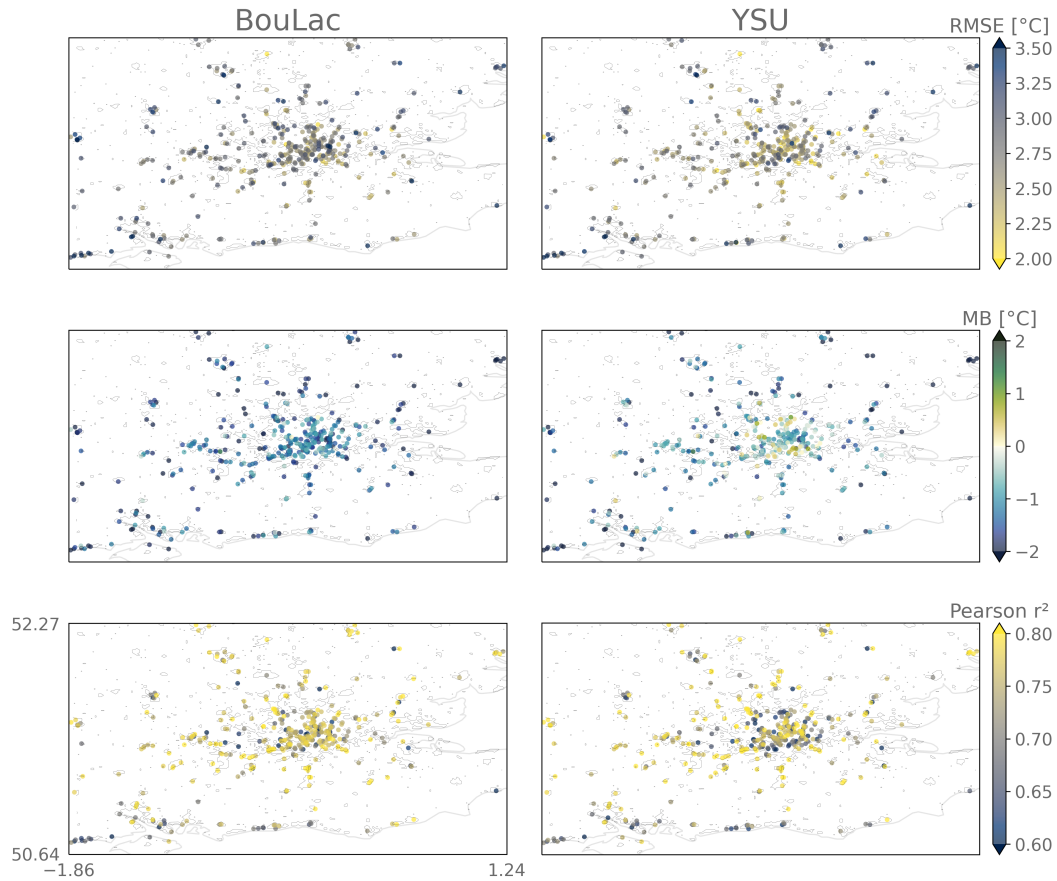


Figure 3. Performance metrics calculated at location of each citizen personal weather station (PWS) for the two model simulations using different planetary boundary layer schemes (YSU and BouLac). The metrics are calculated over the whole summer 2018 with hourly outputs of near surface air temperature at 2 m. Root mean square error (RMSE) and mean bias (MB) are given in degrees Celsius ($^{\circ}\text{C}$). Coefficients of correlation measured with the squared Pearson’s r are also provided. Mean absolute error (MAE) and Spearman’s r are given in Figure B1 to increase clarity.

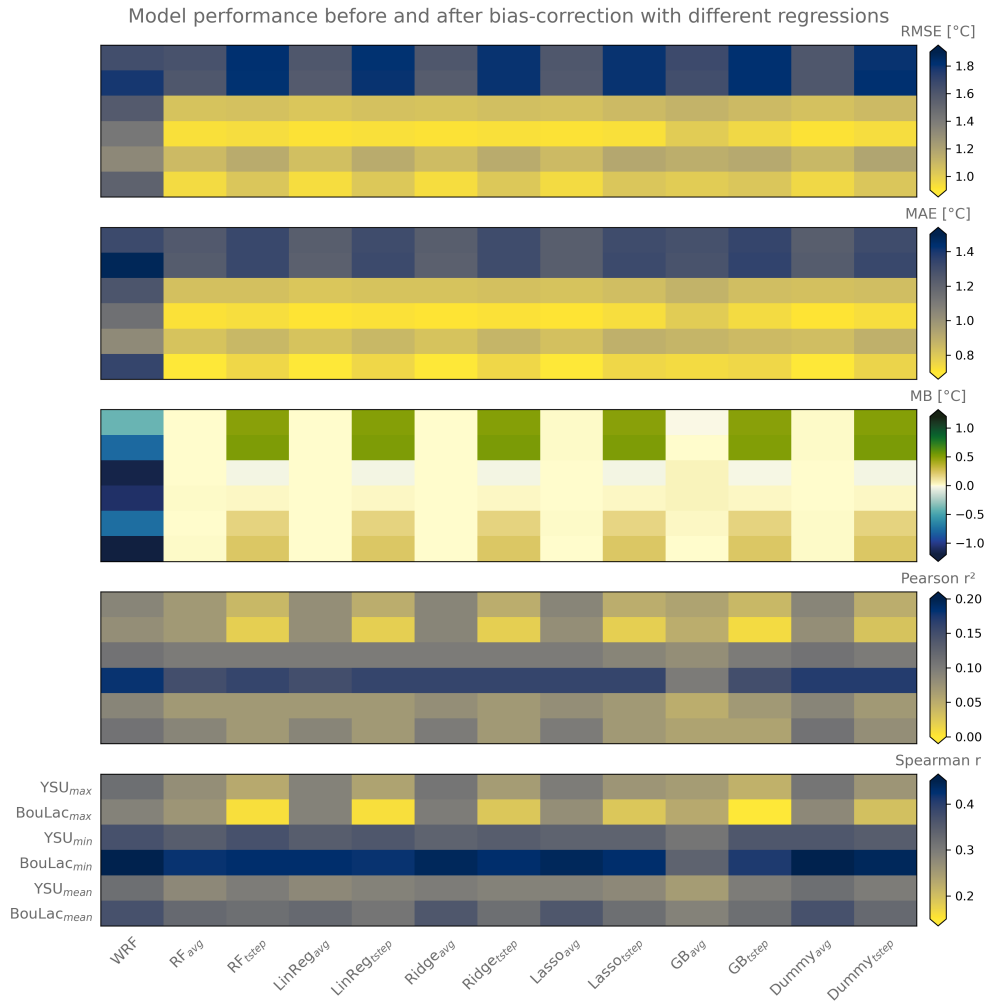


Figure 4. Performance metrics for the model prior to the bias-correction (WRF) and all the different regressions (random forest: RF; linear regression: LinReg; Ridge regression: Ridge; Lasso regression: Lasso; gradient boosting: GB; and dummy regression: Dummy). The different regressions are assigned a suffix: “avg” for regressions that were trained on the summer time-mean average of daily-minimum, -mean or -maximum temperatures, and “tstep” for those that were trained with the temperatures at each daily time-step.

336 After performing a bootstrapping procedure – running the bias-correction 25 times
 337 with 80 % of the CWS as training data and 20 % as testing samples – we can see that each
 338 machine learning regressors give similar performance (Figure 4; values numerically given in
 339 Tables B1 and B2). All bias-corrections were however beneficial compared to the original
 340 outputs from the WRF model, reducing RMSE, MAE and MB by 0.29 °C, 0.32 °C and
 341 1.02 °C on average. The bias-correction was most efficient for daily-minimum temperatures
 342 and less for daily-maximum temperatures, where RMSE was not diminished – if not slightly
 343 increased (by 0.05 °C for YSU daily-maximum temperatures for example) – by the time-
 344 step bias-correction. Interestingly, the spatial correlation between the bias-corrected and the
 345 observed temperatures are low, with values ranging from around 0.02 to 0.2 for the squared
 346 Pearson’s r and from around 0.15 to 0.45 for Spearman’s r . This can be expected as machine
 347 learning algorithms have difficulties representing a time-varying variable with static spatial
 348 elements only (Georganos et al., 2021; Venter et al., 2021). Unexpectedly, we find that the
 349 training at the daily time-step does not outperform the training at the summer time-mean
 350 in terms of spatial correlation with the heat distribution across London. Nonetheless, if
 351 we take the average daily-minimum, -mean and -maximum temperatures of all CWS and
 352 compare it to the modelled temperatures, we find that the time-step bias-correction is closer
 353 to the observations (Figures B2 to B4).

354 Comparing the spatial differences of the bias-corrected products related to the complex-
 355 ities of each regressors, we find that although each regressor is performing similarly on
 356 average, important disparities are found between the outputs. For example, when look-
 357 ing at the average bias-correction imposed to daily-minimum temperatures after training
 358 the regressors at each time-step, the Lasso and the Ridge regressors impose a flat bias-
 359 correction, similar to the dummy regression, while the random forest and gradient boost-
 360 ing regressors’ degrees of freedom result in a spatially diverse bias-correction (Figure 5
 361 and Figures B5 and B6). Besides, the linear regression imposes an average bias-correction
 362 spatially-correlated to the modal LCZ. In general, the signal is consistent across each re-
 363 gressors, apart from the Lasso and the dummy regression, where, for YSU, central London
 364 requires a stronger bias-correction by 1 °C to 2 °C compared to the suburban areas where
 365 the bias-correction is around 0.5 °C ; for BouLac, the central bias-correction is lower than
 366 YSU. We find that these spatial tendencies are also found for daily-maximum and daily-
 367 average temperatures, defending our hypothesis of a systematic bias correlated to spatially
 368 explicit input parameters. The spatial differences in bias-correction are however less impor-
 369 tant for daily-maximum temperatures, which is the time at which the urban heat island is
 370 also expected to be the lowest.

371 Finally, we find that the bias-corrected BouLac simulation corresponds spatially to
 372 predicted temperatures using PWS more than YSU – something we find equally across
 373 all regressors (Figure 6 and Figures B7 to B11). As an example, when comparing the
 374 average bias-corrected products using the time-step trained random forest regressor we can
 375 see that YSU urban heat is more homogeneously distributed than BouLac’s or the predicted
 376 temperatures from PWS only. BouLac’s bias-corrected product shows stronger urban heat
 377 in central London compared to suburban areas, coherent with the predicted temperatures.
 378 Nonetheless, BouLac’s suburban areas are hotter by 0.5 °C to 1.0 °C than the predicted
 379 ones with PWS only. This remains less pronounced than in YSU. Lastly, we can see that
 380 both bias-corrected products show similar trends when compared to the PWS-only predicted
 381 temperatures with hotter suburban areas and cooler secondary cities as well as coastlines.
 382 Again, this does not show which product between the PWS-only predicted temperatures
 383 and the bias-corrected products is better since we do not evaluate this here.

384 These results show that bias-correction of modelled air temperature change their spatio-
 385 temporal distributions. When focusing on the potential impact bias-correction may have
 386 in estimated urban heat impact on urban health, we find that using the random forest
 387 regression trained at each daily time-step leads to an increased average population weighted

Modelled temperatures and respective bias-corrections with multiple regressors

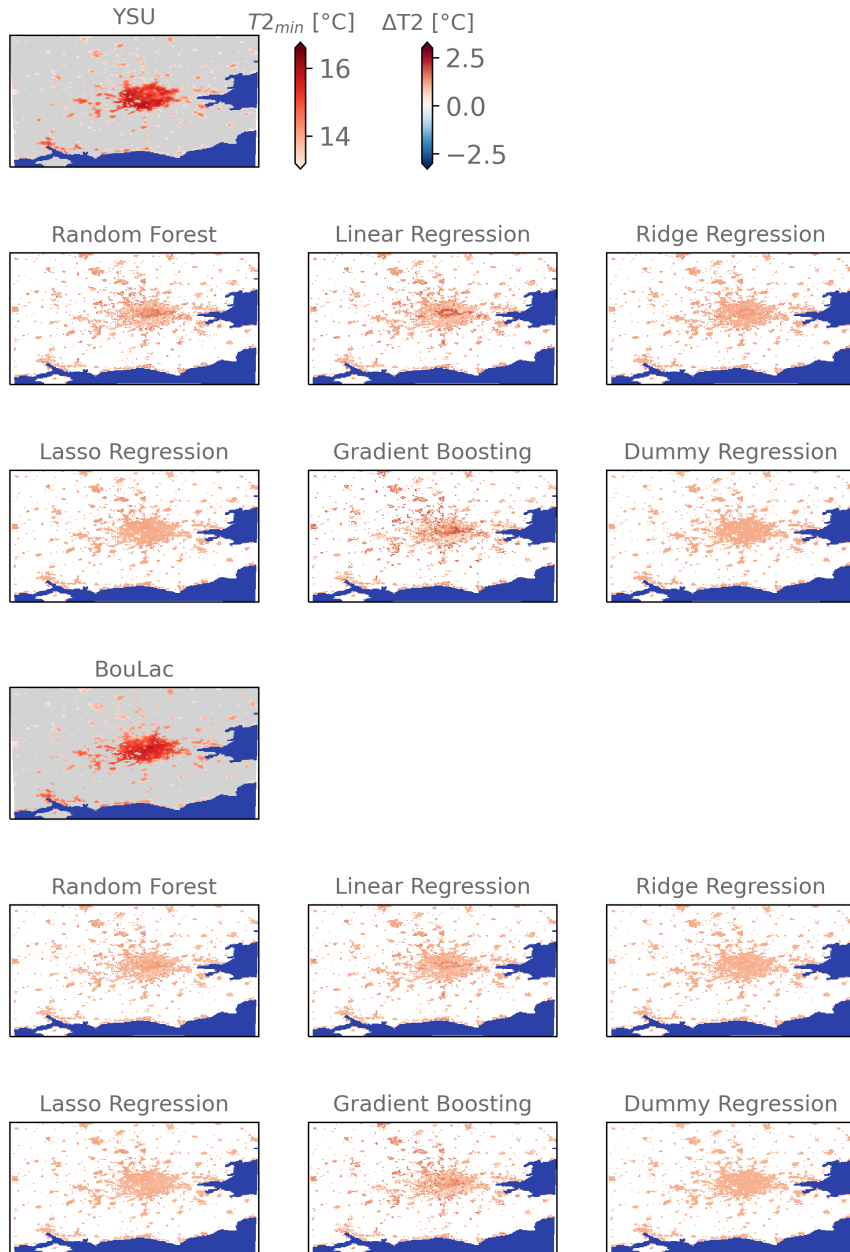


Figure 5. All regressions propose different bias-corrections (ΔT_2) of the average modelled absolute daily minimum urban temperature ($T_{2_{min}}$). Differences of bias-correction are observed between the runs with different planetary boundary layer schemes (Bougeault-Lacarrère – BouLac, and Yonsei University – YSU). The centre of London is subject to a stronger bias-correction. Rural lands are masked in grey and the seas in blue. Bias corrections of daily mean and maximum temperatures are given in Figures B5 and B6

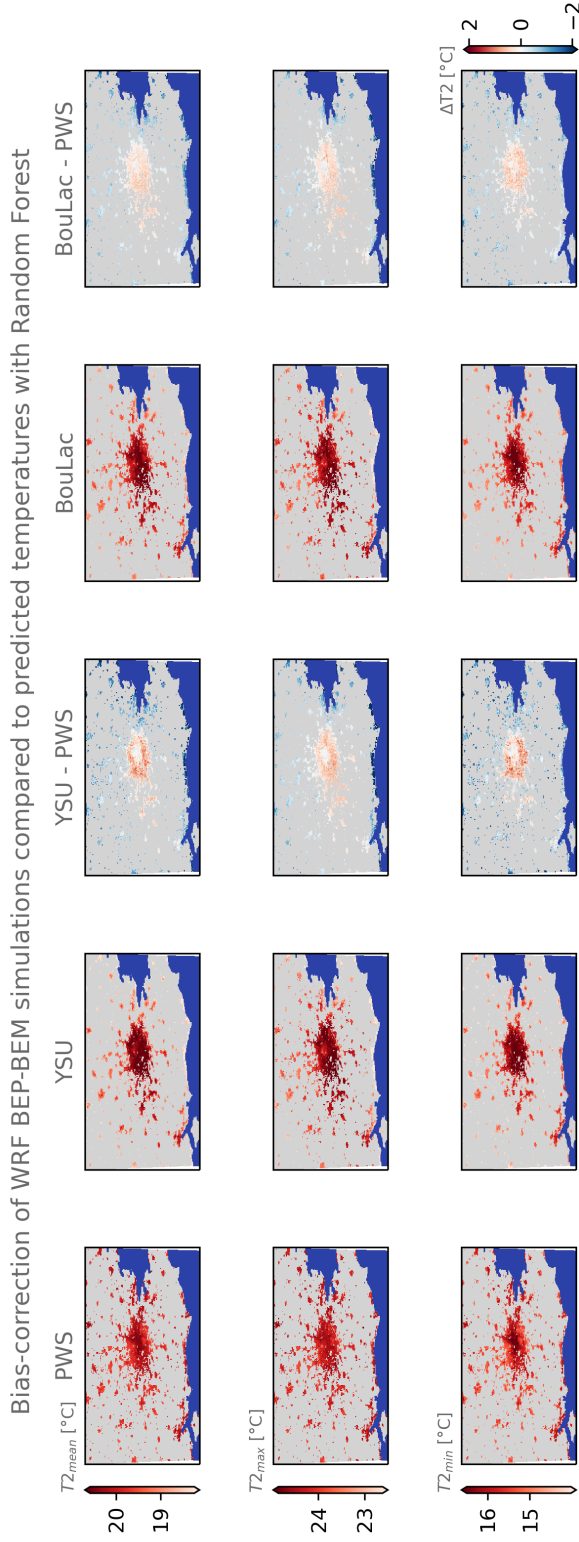


Figure 6. The random forest regressor leads to different bias-corrections of the two WRF simulations parameterized with different turbulence schemes – the Yonsei University (YSU) and the Bougeault-Lacarrère (BouLac) – and with the BEP-BEM urban canopy model activated. This holds for average daily mean, minimum and maximum temperatures ($T2_{mean}$, $T2_{min}$ and $T2_{max}$) after the daily time-step bias-correction. Compared to the predicted temperatures using the personal weather stations data only (PWS), the bias-corrected products are hotter in the suburban areas of the Greater London and cooler in the rural areas. The difference is more pronounced in YSU (see YSU – PWS). Greyed areas represent natural areas where the bias-correction is not performed and the sea is shown in dark blue. The same figures for the other regressors are given in Figures B7 to B11

388 temperature by 0.77 °C in the YSU case, and of 1.24 °C in the BouLac case. Raw model
389 outputs are thereby lowering the impact of heat on the urban population.

390 4 Discussion and conclusions

391 In this study, we argue that the joint use of crowd-sourced personal weather stations
392 (PWS) and urban climate models (UCMs) can add value to urban climate research and in
393 particular to urban climate impact research. This is supported by two major outcomes of our
394 case-study focused over London during the summer 2018. First, we showed that evaluation
395 of urban climate simulations using PWS enables the detection of spatially-varying systematic
396 biases in urban areas related to the UCMs' parameterization, which are not detectable using
397 only official weather stations. Second, we demonstrated that PWS, combined with detailed
398 morphological data derived from LCZ maps, can be used to derive a spatially varying bias-
399 correction via commonly used machine-learning regressors. This latter point has major
400 implications for urban climate impact research – and especially future urban climate impact
401 studies – as we hereby propose the first bias-correction technique that considers the existence
402 of a non-linear spatially heterogeneous bias in modelled urban climates.

403 Of course, using PWS for evaluating UCM simulations should always cautiously be
404 considered because of the lower accuracy of PWS and the potential uncertainties related
405 to user-driven mistakes in the set-up of their PWS (e.g., indoor sensors instead of outdoor,
406 poor shading conditions, height of the sensor, etc.). However, reliable tools have now been
407 developed since the first use of PWS for model evaluation by Hammerberg et al. (2018) to
408 filter dubious measurements out (e.g., Crowd-QC from Napoly et al. (2018) or Crowd-QC +
409 by Fenner et al. (2021)), thus making PWS observations increasingly reliable. This does not
410 resolve the question of the representativity of measurements, i.e., “how is one PWS measure-
411 ment representative of the simulated urban pixel?” Yet, the increasing density of PWS in the
412 urban environments begins to alleviate this uncertainty. For example, Venter et al. (2020)
413 found that a density of one PWS per square kilometre is optimal for predicting seasonal air
414 temperature in Oslo. Dense PWS networks hence permit the detection of systematic biases
415 that would otherwise pass undetected. Therefore, to support the development of PWS as a
416 source of urban weather observations for model evaluation, urban climate scientists should
417 identify an optimal density of PWS for UCM evaluation, to define which cities are in need
418 of urban weather observations, and to start instigating common frameworks and standards.

419 We consider our study innovative and supportive of future advances in the field because
420 it is the first bias-correction technique in urban environments which considers that UCMs'
421 simulated UHI is spatially heterogeneous in its accuracy and that the UHI is not solely
422 linearly correlated to the urban fraction. Aided by the expanding fields of crowd-sourcing
423 weather observations through PWS, machine learning, and potentially deep learning, we
424 infer that our work should serve as the basis of future research that would try, but not re-
425 stricted to, improving the bias-correction of urban climate models using PWS. For instance,
426 we did not find any machine learning regressor to be more efficient at predicting the model
427 bias. This could be explained by the rather restricted set of covariates we used for training
428 the regressors as well as the coarse horizontal resolution of 1 km at which the covariates were
429 aggregated to be consistent with the model's spatial resolution. Higher spatial resolutions
430 and more specific satellite earth observations could be used to improve regressors' perfor-
431 mance, following up on the work by Venter et al. (2021), for example. When modelling the
432 near-surface UHI, which is not a model bias, their regressor achieved similar performances
433 as ours, with an RMSE of 1.05 °C and a Pearson's r^2 of 0.23. Although the common
434 use of model's input parameters and earth observations as covariates could be beneficial, a
435 particular attention should be given to the choice of earth observations since these should
436 not be decorrelated to the model's physics and dynamics as the purpose would remain the
437 bias-correction.

438 Besides, as our results showed by comparing the performance of regressors trained at
439 the daily time-step and with the summer time-mean average, regressors could gain in per-
440 formance by adding a temporal component to the covariates. Following up on this idea,
441 the recent work by (Zunwald et al., 2021) tried predicting the near-surface air temperature
442 in Zurich for the 30th of June 2019 out of ~650 Netatmo PWS' measurements during the
443 preceding week. Their set of covariates consisted of spatial earth observations as well as 35
444 meteorological predictors that were all derived from one official automatic weather stations.
445 The latter predictors helped training the model to recognise how the temperature measured
446 at each PWS location was related to the meteorological variables measured at the automatic
447 weather stations. Their predictions at hourly time-steps achieved reasonable performances
448 with RMSEs around 1.70 °C. Bias-correction of UCM simulations could hence be improved
449 by incorporating temporally explicit meteorological observations from official weather sta-
450 tions. Notwithstanding, this would require extensive investigation on the area down to
451 which each official station is representative for training the regressors. More geographically
452 oriented machine learning regressors, like the geographical random forests (Georganos et al.,
453 2021), could also help integrate these spatial heterogeneities for an improved bias-correction.

454 In general, we support the use of quality-controlled PWS observations for bias-correction
455 of urban climate simulations. As shown in this case study, model outputs prior to any bias-
456 correction could lead to under- or over-estimation of urban heat impact on public health.
457 We indeed find that for the summer 2018 in London, average population weighted temper-
458 atures were higher after bias-correcting the model outputs, suggesting higher urban heat
459 related mortality during this period. This simple example shows that bias-correction of
460 urban climate simulations could have important implications for calculating the exposure of
461 urban citizen to heat or estimating the urban heat-related mortality. Although preferring
462 bias-corrected model outputs to predicted urban air temperatures from earth observations
463 for present-day urban heat impact studies is not covered in this study – and must be further
464 explored – we still argue that bias-correction should be done prior to any urban heat impact
465 studies that imply using climate model outputs. This argument is especially valid for future
466 climate projections at urban scale and we encourage future research to investigate how to
467 transfer present urban bias-correction coefficients to simulated future urban climates. Doing
468 so, bias-corrected simulations could help targeting areas where heat mitigation or adapta-
469 tion strategies could be more beneficial as their efficiency is dependent on their location and
470 scales of implementation (J. Yang & Bou-Zeid, 2019; Broadbent et al., 2022).

471 5 Open Research

472 The simulations done in this research were performed using the WRF model v4.3
473 (<https://github.com/wrf-model/WRF.git>). The related outputs presented in this re-
474 search are available upon reasonable request addressed to the corresponding author.

475 Acknowledgments

476
477 We personally thank Stefanos Georganos for his help and his comments on machine
478 learning classifiers and regressors. We also thank Daniel Fenner and Fred Meier for their
479 valuable insights concerning data acquisition, filtering and treatment of crowd-sourced citi-
480 zen weather stations. Lastly, we are grateful to Matthias Demuzere and other committed
481 members of the WUDAPT project for providing the European LCZ map and the python
482 W2W tools. CH is supported by a NERC fellowship (NE/R01440X/1) and acknowledges
483 funding for the HEROIC project (216035/Z/19/Z) from the Wellcome Trust, which funds
484 OB and CS.

485 OB designed the study and led the conception of the manuscript with the support of
486 CH and CS. OB was responsible for the WRF modelling, the model evaluation and the

487 bias-correction. CS provided support in the python coding and in the statistical analysis for
488 the bias-correction. OK was responsible for technical support of the installation of WRF on
489 the University College London's "Kathleen" and "Myriad" super-computers. AZ and AM
490 offered guidance in the set-up of the WRF model v4.3 and urban heat modelling expertise
491 with SK. All authors contributed to the writing of the manuscript.

492 The authors declare no conflicts of interest.

References

493

494

495

496

497

498

499

500

501

502

503

504

505

506

507

508

509

510

511

512

513

514

515

516

517

518

519

520

521

522

523

524

525

526

527

528

529

530

531

532

533

534

535

536

537

538

539

540

541

542

543

544

545

546

547

- Bassett, R., Young, P., Blair, G., Samreen, F., & Simm, W. (2020). A large ensemble approach to quantifying internal model variability within the wrf numerical model. *Journal of Geophysical Research: Atmospheres*, *125*(7), e2019JD031286.
- Benjamin, K., Luo, Z., & Wang, X. (2021). Crowdsourcing urban air temperature data for estimating urban heat island and building heating/cooling load in london. *Energies*, *14*(16), 5208.
- Bougeault, P., & Lacarrere, P. (1989). Parameterization of orography-induced turbulence in a mesobeta-scale model. *Monthly weather review*, *117*(8), 1872–1890.
- Brisson, E., Demuzere, M., & Van Lipzig, N. (2015). Modelling strategies for performing convection-permitting climate simulations. *Meteorologische Zeitschrift*, *25*(2), 149–163.
- Broadbent, A. M., Declet-Barreto, J., Krayenhoff, E. S., Harlan, S. L., & Georgescu, M. (2022). Targeted implementation of cool roofs for equitable urban adaptation to extreme heat. *Science of the Total Environment*, *811*, 151326.
- Brousse, O., Martilli, A., Foley, M., Mills, G., & Bechtel, B. (2016). Wudapt, an efficient land use producing data tool for mesoscale models? integration of urban lcz in wrf over madrid. *Urban Climate*, *17*, 116–134.
- Brousse, O., Simpson, C., Walker, N., Fenner, D., Meier, F., Taylor, J., & Heaviside, C. (2022). Evidence of horizontal urban heat advection in london using six years of data from a citizen weather station network. *Environmental Research Letters*, *17*(4), 044041.
- Chapman, L., Bell, C., & Bell, S. (2017). Can the crowdsourcing data paradigm take atmospheric science to a new level? a case study of the urban heat island of london quantified using netatmo weather stations. *International Journal of Climatology*, *37*(9), 3597–3605.
- Ching, J., Mills, G., Bechtel, B., See, L., Feddema, J., Wang, X., ... others (2018). Wudapt: An urban weather, climate, and environmental modeling infrastructure for the anthropocene. *Bulletin of the American Meteorological Society*, *99*(9), 1907–1924.
- Demuzere, M., Argüeso, D., Zonato, A., & Kittner, J. (2021). *W2w: A python package that injects wudapt's local climate zone information in wrf (version v0.1.1)*. (retrieved online, <https://pypi.org/project/w2w/>)
- Demuzere, M., Bechtel, B., Middel, A., & Mills, G. (2019). Mapping europe into local climate zones. *PloS one*, *14*(4), e0214474.
- Demuzere, M., Harshan, S., Järvi, L., Roth, M., Grimmond, C., Masson, V., ... Wouters, H. (2017). Impact of urban canopy models and external parameters on the modelled urban energy balance in a tropical city. *Quarterly Journal of the Royal Meteorological Society*, *143*(704), 1581–1596.
- Demuzere, M., Kittner, J., Martilli, A., Mills, G., Moede, C., Stewart, I. D., ... Bechtel, B. (2022). A global map of local climate zones to support earth system modelling and urban scale environmental science. *Earth System Science Data Discussions*, 1–57.
- Dudhia, J. (1989). Numerical study of convection observed during the winter monsoon experiment using a mesoscale two-dimensional model. *Journal of Atmospheric Sciences*, *46*(20), 3077–3107.
- Fenner, D., Bechtel, B., Demuzere, M., Kittner, J., & Meier, F. (2021). Crowdqc+—a quality-control for crowdsourced air-temperature observations enabling world-wide urban climate applications. *Frontiers in Environmental Science*, 553.
- Fenner, D., Holtmann, A., Meier, F., Langer, I., & Scherer, D. (2019). Contrasting changes of urban heat island intensity during hot weather episodes. *Environmental Research Letters*, *14*(12), 124013.
- Fenner, D., Meier, F., Bechtel, B., Otto, M., & Scherer, D. (2017). Intra and inter ‘local climate zone’ variability of air temperature as observed by crowdsourced citizen weather stations in berlin, germany. *10.14279/depositonce-10378*.
- Georganos, S., Grippa, T., Niang Gadiaga, A., Linard, C., Lennert, M., Vanhuyse, S., ... Kalogirou, S. (2021). Geographical random forests: a spatial extension of the random

- 548 forest algorithm to address spatial heterogeneity in remote sensing and population
 549 modelling. *Geocarto International*, *36*(2), 121–136.
- 550 Grassmann, T., Napoly, A., Meier, F., & Fenner, D. (2018). Quality control for crowdsourced
 551 data from cws.
- 552 Grimmond, C. S. B., Blackett, M., Best, M. J., Baik, J.-J., Belcher, S., Beringer, J., ...
 553 others (2011). Initial results from phase 2 of the international urban energy balance
 554 model comparison. *International Journal of Climatology*, *31*(2), 244–272.
- 555 Gutiérrez, E., González, J. E., Martilli, A., Bornstein, R., & Arend, M. (2015). Simulations
 556 of a heat-wave event in new york city using a multilayer urban parameterization.
 557 *Journal of Applied Meteorology and Climatology*, *54*(2), 283–301.
- 558 Hammerberg, K., Brousse, O., Martilli, A., & Mahdavi, A. (2018). Implications of employing
 559 detailed urban canopy parameters for mesoscale climate modelling: a comparison
 560 between wudapt and gis databases over vienna, austria. *International Journal of
 561 Climatology*, *38*, e1241–e1257.
- 562 Heaviside, C., Cai, X.-M., & Vardoulakis, S. (2015). The effects of horizontal advection on
 563 the urban heat island in birmingham and the west midlands, united kingdom during
 564 a heatwave. *Quarterly Journal of the Royal Meteorological Society*, *141*(689), 1429–
 565 1441.
- 566 Hendricks, E. A., Knievel, J. C., & Wang, Y. (2020). Addition of multilayer urban canopy
 567 models to a nonlocal planetary boundary layer parameterization and evaluation using
 568 ideal and real cases. *Journal of Applied Meteorology and Climatology*, *59*(8), 1369–
 569 1392.
- 570 Hollis, D., McCarthy, M., Kendon, M., Legg, T., & Simpson, I. (2019). Haduk-grid—a new
 571 uk dataset of gridded climate observations. *Geoscience Data Journal*, *6*(2), 151–159.
- 572 Hong, S.-Y., Dudhia, J., & Chen, S.-H. (2004). A revised approach to ice microphysical
 573 processes for the bulk parameterization of clouds and precipitation. *Monthly weather
 574 review*, *132*(1), 103–120.
- 575 Hong, S.-Y., & Kim, S.-W. (2008). Stable boundary layer mixing in a vertical diffusion
 576 scheme. In *18th symposium on boundary layers and turbulence b* (Vol. 16, p. 325).
- 577 Hong, S.-Y., Noh, Y., & Dudhia, J. (2006). A new vertical diffusion package with an explicit
 578 treatment of entrainment processes. *Monthly weather review*, *134*(9), 2318–2341.
- 579 Janjić, Z. I. (2001). Nonsingular implementation of the mellor-yamada level 2.5 scheme in
 580 the ncep meso model.
- 581 Janjić, Z. I. (1994). The step-mountain eta coordinate model: Further developments of
 582 the convection, viscous sublayer, and turbulence closure schemes. *Monthly weather
 583 review*, *122*(5), 927–945.
- 584 Jiménez, P. A., Dudhia, J., González-Rouco, J. F., Navarro, J., Montávez, J. P., & García-
 585 Bustamante, E. (2012). A revised scheme for the wrf surface layer formulation.
 586 *Monthly weather review*, *140*(3), 898–918.
- 587 Kain, J. S. (2004). The kain–fritsch convective parameterization: an update. *Journal of
 588 applied meteorology*, *43*(1), 170–181.
- 589 Lauwaet, D., Hooyberghs, H., Maiheu, B., Lefebvre, W., Driesen, G., Van Looy, S., &
 590 De Ridder, K. (2015). Detailed urban heat island projections for cities worldwide:
 591 dynamical downscaling cmip5 global climate models. *Climate*, *3*(2), 391–415.
- 592 Lipson, M., Grimmond, S., & Best, M. (2021). Urban-plumber model evaluation project:
 593 initial results. In *Egu general assembly conference abstracts* (pp. EGU21–15230).
- 594 Loridan, T., & Grimmond, C. (2012). Multi-site evaluation of an urban land-surface model:
 595 Intra-urban heterogeneity, seasonality and parameter complexity requirements. *Quar-
 596 terly Journal of the Royal Meteorological Society*, *138*(665), 1094–1113.
- 597 Maraun, D., & Widmann, M. (2018). *Statistical downscaling and bias correction for climate
 598 research*. Cambridge University Press.
- 599 Martilli, A., Clappier, A., & Rotach, M. W. (2002). An urban surface exchange parameter-
 600 isation for mesoscale models. *Boundary-layer meteorology*, *104*(2), 261–304.
- 601 Martilli, A., Sanchez, B., Rasilla, D., Pappacogli, G., Allende, F., Martin, F., ... Fer-
 602 nandez, F. (2021). Simulating the meteorology during persistent wintertime thermal

- 603 inversions over urban areas. the case of madrid. *Atmospheric Research*, *263*, 105789.
- 604 Masson, V. (2000). A physically-based scheme for the urban energy budget in atmospheric
605 models. *Boundary-layer meteorology*, *94*(3), 357–397.
- 606 McCarthy, M., Christidis, N., Dunstone, N., Fereday, D., Kay, G., Klein-Tank, A., . . . Stott,
607 P. (2019). Drivers of the uk summer heatwave of 2018. *Weather*, *74*(11), 390–396.
- 608 Meier, F., Fenner, D., Grassmann, T., Otto, M., & Scherer, D. (2017). Crowdsourcing air
609 temperature from citizen weather stations for urban climate research. *Urban Climate*,
610 *19*, 170–191.
- 611 Mlawer, E. J., Taubman, S. J., Brown, P. D., Iacono, M. J., & Clough, S. A. (1997).
612 Radiative transfer for inhomogeneous atmospheres: Rrtm, a validated correlated-k
613 model for the longwave. *Journal of Geophysical Research: Atmospheres*, *102*(D14),
614 16663–16682.
- 615 Mughal, M. O., Li, X.-X., Yin, T., Martilli, A., Brousse, O., Dissegna, M. A., & Norford,
616 L. K. (2019). High-resolution, multilayer modeling of singapore’s urban climate incor-
617 porating local climate zones. *Journal of Geophysical Research: Atmospheres*, *124*(14),
618 7764–7785.
- 619 Muller, C., Chapman, L., Johnston, S., Kidd, C., Illingworth, S., Foody, G., . . . Leigh,
620 R. (2015). Crowdsourcing for climate and atmospheric sciences: current status and
621 future potential. *International Journal of Climatology*, *35*(11), 3185–3203.
- 622 Napoly, A., Grassmann, T., Meier, F., & Fenner, D. (2018). Development and application of
623 a statistically-based quality control for crowdsourced air temperature data. *Frontiers*
624 *in Earth Science*, *6*, 118.
- 625 Nazarian, N., Krayenhoff, S., Bechtel, B., Hondula, D., Paolini, R., Vanos, J. K., . . . others
626 (2022). Integrated assessment of urban overheating impacts on human life. *Earth’s*
627 *Future*.
- 628 Niu, G.-Y., Yang, Z.-L., Mitchell, K. E., Chen, F., Ek, M. B., Barlage, M., . . . others (2011).
629 The community noah land surface model with multiparameterization options (noah-
630 mp): 1. model description and evaluation with local-scale measurements. *Journal of*
631 *Geophysical Research: Atmospheres*, *116*(D12).
- 632 Oke, T. R., Mills, G., Christen, A., & Voogt, J. A. (2017). *Urban climates*. Cambridge
633 University Press.
- 634 Oleson, K., Anderson, G., Jones, B., McGinnis, S., & Sanderson, B. (2018). Avoided climate
635 impacts of urban and rural heat and cold waves over the us using large climate model
636 ensembles for rcp8. 5 and rcp4. 5. *Climatic change*, *146*(3), 377–392.
- 637 Pedregosa, F., Varoquaux, G., Gramfort, A., Michel, V., Thirion, B., Grisel, O., . . . others
638 (2011). Scikit-learn: Machine learning in python. *the Journal of machine Learning*
639 *research*, *12*, 2825–2830.
- 640 Potgieter, J., Nazarian, N., Lipson, M. J., Hart, M. A., Ulpiani, G., Morrison, W., &
641 Benjamin, K. (2021). Combining high-resolution land use data with crowdsourced
642 air temperature to investigate intra-urban microclimate. *Frontiers in Environmental*
643 *Science*, 385.
- 644 Salamanca, F., Krpo, A., Martilli, A., & Clappier, A. (2010). A new building energy model
645 coupled with an urban canopy parameterization for urban climate simulations—part i.
646 formulation, verification, and sensitivity analysis of the model. *Theoretical and applied*
647 *climatology*, *99*(3), 331–344.
- 648 Salamanca, F., & Martilli, A. (2010). A new building energy model coupled with an urban
649 canopy parameterization for urban climate simulations—part ii. validation with one
650 dimension off-line simulations. *Theoretical and Applied Climatology*, *99*(3), 345–356.
- 651 Salamanca, F., Martilli, A., Tewari, M., & Chen, F. (2011). A study of the urban bound-
652 ary layer using different urban parameterizations and high-resolution urban canopy
653 parameters with wrf. *Journal of Applied Meteorology and Climatology*, *50*(5), 1107–
654 1128.
- 655 Salamanca, F., Martilli, A., & Yagüe, C. (2012). A numerical study of the urban heat island
656 over madrid during the desirex (2008) campaign with wrf and an evaluation of simple
657 mitigation strategies. *International Journal of Climatology*, *32*(15), 2372–2386.

- 658 Sgoff, C., Acevedo, W., Paschalidi, Z., Ulbrich, S., Bauernschubert, E., Kratzsch, T., &
659 Potthast, R. (2022). Assimilation of crowd-sourced surface observations over germany
660 in a regional weather prediction system. *Quarterly Journal of the Royal Meteorological
661 Society*.
- 662 Stewart, I. D., & Oke, T. R. (2012). Local climate zones for urban temperature studies.
663 *Bulletin of the American Meteorological Society*, *93*(12), 1879–1900.
- 664 Stewart, I. D., Oke, T. R., & Krayenhoff, E. S. (2014). Evaluation of the ‘local climate
665 zone’ scheme using temperature observations and model simulations. *International
666 journal of climatology*, *34*(4), 1062–1080.
- 667 Sunter, M. (2021). Midas data user guide for uk land observations, v20210705.
- 668 Tewari, M., Salamanca, F., Martilli, A., Treinish, L., & Mahalov, A. (2017). Impacts
669 of projected urban expansion and global warming on cooling energy demand over a
670 semiarid region. *Atmospheric Science Letters*, *18*(11), 419–426.
- 671 UKMO. (2021). *Midas open: Uk hourly weather observation data, v202107*. centre for
672 *environmental data analysis, 08 september 2021*. (data retrieved online, doi:10.5285/
673 3bd7221d4844435dad2fa030f26ab5fd)
- 674 Varentsov, M., Fenner, D., Meier, F., Samsonov, T., & Demuzere, M. (2021). Quantifying
675 local and mesoscale drivers of the urban heat island of moscow with reference and
676 crowdsourced observations. *Frontiers in Environmental Science*, 543.
- 677 Venter, Z. S., Brousse, O., Esau, I., & Meier, F. (2020). Hyperlocal mapping of urban air
678 temperature using remote sensing and crowdsourced weather data. *Remote Sensing
679 of Environment*, *242*, 111791.
- 680 Venter, Z. S., Chakraborty, T., & Lee, X. (2021). Crowdsourced air temperatures contrast
681 satellite measures of the urban heat island and its mechanisms. *Science Advances*,
682 *7*(22), eabb9569.
- 683 Virtanen, P., Gommers, R., Oliphant, T. E., Haberland, M., Reddy, T., Cournapeau, D., ...
684 others (2020). Scipy 1.0: fundamental algorithms for scientific computing in python.
685 *Nature methods*, *17*(3), 261–272.
- 686 Wang, J., & Hu, X.-M. (2021). Evaluating the performance of wrf urban schemes and pbl
687 schemes over dallas–fort worth during a dry summer and a wet summer. *Journal of
688 Applied Meteorology and Climatology*, *60*(6), 779–798.
- 689 Wouters, H., Demuzere, M., Blahak, U., Fortuniak, K., Maiheu, B., Camps, J., ... van
690 Lipzig, N. P. (2016). The efficient urban canopy dependency parametrization (sury)
691 v1.0 for atmospheric modelling: description and application with the cosmo-clm model
692 for a belgian summer. *Geoscientific Model Development*, *9*(9), 3027–3054.
- 693 Wouters, H., De Ridder, K., Poelmans, L., Willems, P., Brouwers, J., Hosseinzadehtalaei,
694 P., ... Demuzere, M. (2017). Heat stress increase under climate change twice as
695 large in cities as in rural areas: A study for a densely populated midlatitude maritime
696 region. *Geophysical Research Letters*, *44*(17), 8997–9007.
- 697 Yang, J., & Bou-Zeid, E. (2019). Scale dependence of the benefits and efficiency of green
698 and cool roofs. *Landscape and urban planning*, *185*, 127–140.
- 699 Yang, Z.-L., Niu, G.-Y., Mitchell, K. E., Chen, F., Ek, M. B., Barlage, M., ... others
700 (2011). The community noah land surface model with multiparameterization options
701 (noah-mp): 2. evaluation over global river basins. *Journal of Geophysical Research:
702 Atmospheres*, *116*(D12).
- 703 Zängl, G., Reinert, D., Rípodas, P., & Baldauf, M. (2015). The icon (icosahedral
704 non-hydrostatic) modelling framework of dwd and mpi-m: Description of the non-
705 hydrostatic dynamical core. *Quarterly Journal of the Royal Meteorological Society*,
706 *141*(687), 563–579.
- 707 Zonato, A., Martilli, A., Di Sabatino, S., Zardi, D., & Giovannini, L. (2020). Evaluating
708 the performance of a novel wudapt averaging technique to define urban morphology
709 with mesoscale models. *Urban Climate*, *31*, 100584.
- 710 Zonato, A., Martilli, A., Jimenez, P. A., Dudhia, J., Zardi, D., & Giovannini, L. (2022). A
711 new $k-\epsilon$ turbulence parameterization for mesoscale meteorological models. *Monthly
712 Weather Review*.

713 Zumwald, M., Knüsel, B., Bresch, D. N., & Knutti, R. (2021). Mapping urban temperature
714 using crowd-sensing data and machine learning. *Urban Climate*, 35, 100739.

Appendix A Model sensitivity testing over the two hottest days of Summer 2018

Prior to running the 3-months simulation, we tested the model's sensitivity to a set of parameterization to assess which model is the best performing model for the 3-months simulation. We perform the sensitivity in a progressive way; parameters are kept if beneficial, removed if detrimental. We chose to run the simulations over the two hottest days of the summer 2018 with one additional day as spin-up time – from the 25th to the 27th of July 2018 – to see how the model is capable of accurately representing an extreme condition in terms of air temperature at 2 m – tested against official MIDAS automatic weather stations and personal Netatmo PWS. The model was also tested for relative humidity and wind speed at 10 m at MIDAS locations where records were available. All wind-speed measurements are converted from knots to $\text{m}\cdot\text{s}^{-1}$.

We start from Heaviside et al. (2015) model's parameterization, who simulated the impact of urbanization on the local climate in the West Midlands in England, but supplement the CORINE land-use land-cover by the Local Climate Zones classification instead since Brousse et al. (2016) compared both products and proved the added value of LCZ over Madrid. We chose the work by Heaviside et al. (2015) as a starting point since it also uses the BEP urban climate model, coupled to the WRF model and is one of the only WRF simulations done over England.

From there, our simulations tested: i) the use of YSU, recently coupled to the BEP-BEM model (Hendricks et al., 2020), instead of Bougeault-Lacarrere; ii) the use of the more complex land surface scheme Noah-MP in its default parameterization instead of the default Noah land surface model; iii) the forcing by ERA5 reanalysis data at 25 km horizontal resolution instead of ERA-Interim; iv) the reduction of soil moisture by 50 % and its increase by 200 %, following suggestions provided by Martilli et al. (2021). We chose not to test the impact of urban canopy parameters in this case to keep our simulations standardized and universally coherent through the LCZ scheme. Their simulation used the same micro-, clouds, convection and radiation physics than ours.

We found that all steps taken from the original parameterization by Heaviside et al. (2015) were beneficial to the model's performance. Through an intermediate simulation where we tested again the BouLac turbulence scheme after step iii, we found that YSU was still performing better.

Appendix B Additional Figures and Tables

This section presents all the figures that are not given in the main text.

Table B1. Performance metrics used in Figure 4 for the model using BouLac prior to the bias-correction (WRF) and all the different regressors (random forest: RF; linear regression: LR; Ridge regression: RD; Lasso regression: LA; gradient boosting: GB; and dummy regression: DU). The different regressions are assigned a suffix: “avg” for regressions that were trained on the summer time-mean average of daily-minimum, -mean or -maximum temperatures, and “tstep” for those that were trained with the temperatures at each daily time-step.

BouLac													
	WRF	RF_{avg}	RF_{tstep}	LR_{avg}	LR_{tstep}	RD_{avg}	RD_{tstep}	LA_{avg}	LA_{tstep}	GB_{avg}	GB_{tstep}	DU_{avg}	DU_{tstep}
MEAN													
RMSE	1.54	0.95	1.04	0.94	1.03	0.94	1.03	0.95	1.04	1.01	1.04	0.96	1.04
MAE	1.34	0.69	0.75	0.69	0.75	0.68	0.75	0.69	0.75	0.74	0.75	0.7	0.76
MB	-1.2	0.01	0.23	0	0.23	0	0.23	0	0.23	0	0.23	0.01	0.23
Pearson r²	0.11	0.09	0.07	0.09	0.07	0.1	0.07	0.1	0.07	0.06	0.06	0.11	0.08
Spearman r	0.37	0.33	0.32	0.33	0.31	0.36	0.32	0.36	0.32	0.29	0.32	0.37	0.33 0.88
MIN													
RMSE	1.42	0.93	0.94	0.92	0.93	0.92	0.93	0.92	0.93	1.01	0.96	0.92	0.94
MAE	1.15	0.72	0.73	0.71	0.72	0.71	0.72	0.71	0.73	0.79	0.74	0.71	0.73
MB	-1.08	0.01	0.02	0	0.02	0	0.02	0	0.02	0.04	0.02	0	0.02
Pearson r²	0.18	0.15	0.16	0.15	0.16	0.16	0.16	0.16	0.16	0.1	0.15	0.17	0.17
Spearman r	0.46	0.42	0.43	0.43	0.42	0.44	0.43	0.44	0.43	0.34	0.41	0.46	0.44
MAX													
RMSE	1.78	1.6	1.81	1.58	1.8	1.57	1.8	1.59	1.8	1.65	1.82	1.6	1.82
MAE	1.48	1.24	1.33	1.22	1.32	1.22	1.31	1.23	1.32	1.28	1.35	1.24	1.33
MB	-0.79	0	0.52	0	0.52	0	0.53	0.01	0.52	0	0.51	0.01	0.53
Spearman r	0.08	0.07	0.02	0.08	0.02	0.09	0.02	0.08	0.02	0.05	0.01	0.08	0.03
Spearman r	0.29	0.26	0.16	0.29	0.16	0.3	0.19	0.27	0.19	0.23	0.14	0.28	0.2

Table B2. Performance metrics used in Figure 4 for the model using YSU prior to the bias-correction (WRF) and all the different regressors (random forest: RF; linear regression: LR; Ridge regression: RD; Lasso regression: LA; gradient boosting: GB; and dummy regression: DU). The different regressions are assigned a suffix: “avg” for regressions that were trained on the summer time-mean average of daily-minimum, -mean or -maximum temperatures, and “tstep” for those that were trained with the temperatures at each daily time-step.

	WRF	RF _{avg}	RF _{tstep}	LR _{avg}	LR _{tstep}	RD _{avg}	RD _{tstep}	LA _{avg}	LA _{tstep}	GB _{avg}	GB _{tstep}	DU _{avg}	DU _{tstep}
YSU													
MEAN													
RMSE	1.33	1.09	1.16	1.07	1.16	1.08	1.16	1.09	1.18	1.15	1.17	1.1	1.19
MAE	1.04	0.82	0.86	0.82	0.86	0.82	0.87	0.83	0.89	0.87	0.85	0.84	0.89
MB	-0.76	0	0.17	0	0.17	0	0.17	0.01	0.16	0.02	0.17	0.01	0.17
Pearson r^2	0.09	0.07	0.07	0.07	0.07	0.08	0.07	0.08	0.07	0.05	0.07	0.09	0.07
Spearman r	0.32	0.28	0.3	0.28	0.29	0.3	0.29	0.29	0.28	0.25	0.3	0.32	0.3
MIN													
RMSE	1.58	1.05	1.06	1.04	1.06	1.05	1.07	1.06	1.09	1.12	1.09	1.06	1.09
MAE	1.27	0.83	0.83	0.81	0.82	0.82	0.83	0.82	0.84	0.88	0.84	0.83	0.84
MB	-1.17	0	-0.03	0	-0.03	0	-0.03	0	-0.03	0.04	-0.02	0	-0.03
Pearson r^2	0.11	0.1	0.1	0.1	0.1	0.1	0.1	0.1	0.09	0.08	0.1	0.11	0.1
Spearman r	0.37	0.35	0.37	0.35	0.36	0.34	0.35	0.34	0.34	0.31	0.36	0.36	0.35
MAX													
RMSE	1.65	1.63	1.82	1.6	1.81	1.6	1.8	1.6	1.8	1.67	1.82	1.6	1.8
MAE	1.32	1.25	1.33	1.23	1.31	1.23	1.31	1.23	1.31	1.29	1.34	1.23	1.31
MB	-0.41	0	0.49	0	0.5	0	0.5	0.01	0.49	-0.01	0.49	0.01	0.5
Pearson r^2	0.09	0.07	0.04	0.08	0.05	0.09	0.05	0.09	0.05	0.06	0.04	0.09	0.05
Spearman r	0.32	0.27	0.23	0.29	0.24	0.31	0.25	0.3	0.26	0.25	0.22	0.31	0.26

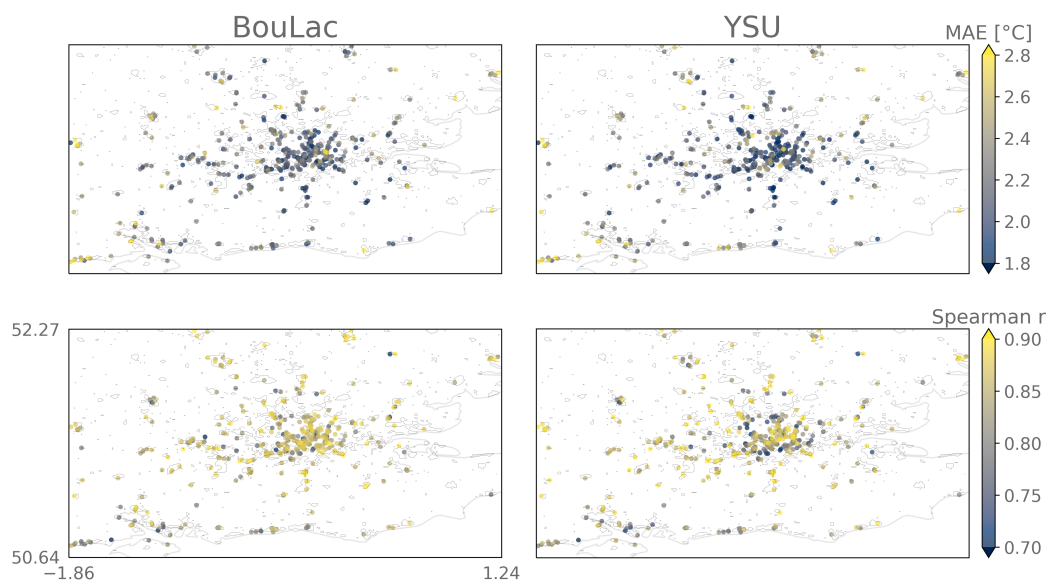


Figure B1. Same as figure 3, but for MAE and Spearman's r .

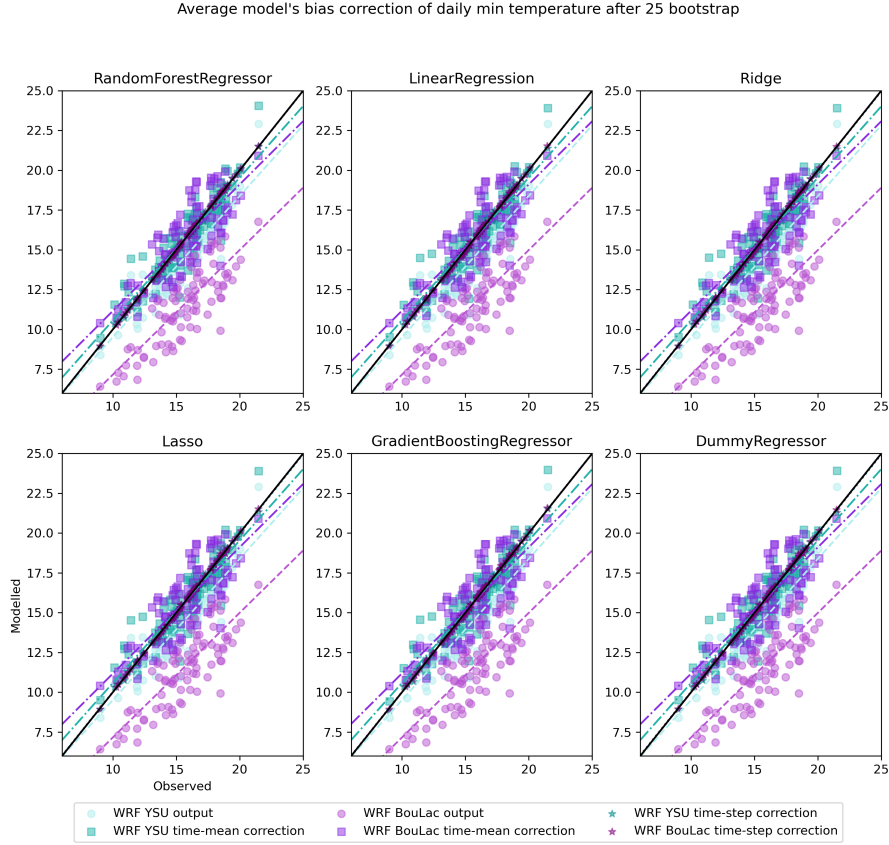


Figure B2. Average modelled daily minimum air temperature at 2 m against observed at citizens' personal weather stations locations show that all machine learning regressors perform a similar bias-correction on average. In blue, modelled temperatures at 2 m are from the model simulation that used the Yonsei University (YSU) planetary boundary layer scheme before the bias correction (circles), after the summer time-mean bias correction (squares) and after the daily time-step bias correction (stars). In purple, the same values are given for the simulation which used the Bougeault-Lacarrère (BouLac) scheme. Dashed lines represent the least squares polynomial fitted lines and the black full line represents the identity line.

Average model's bias correction of daily max temperature after 25 bootstrap

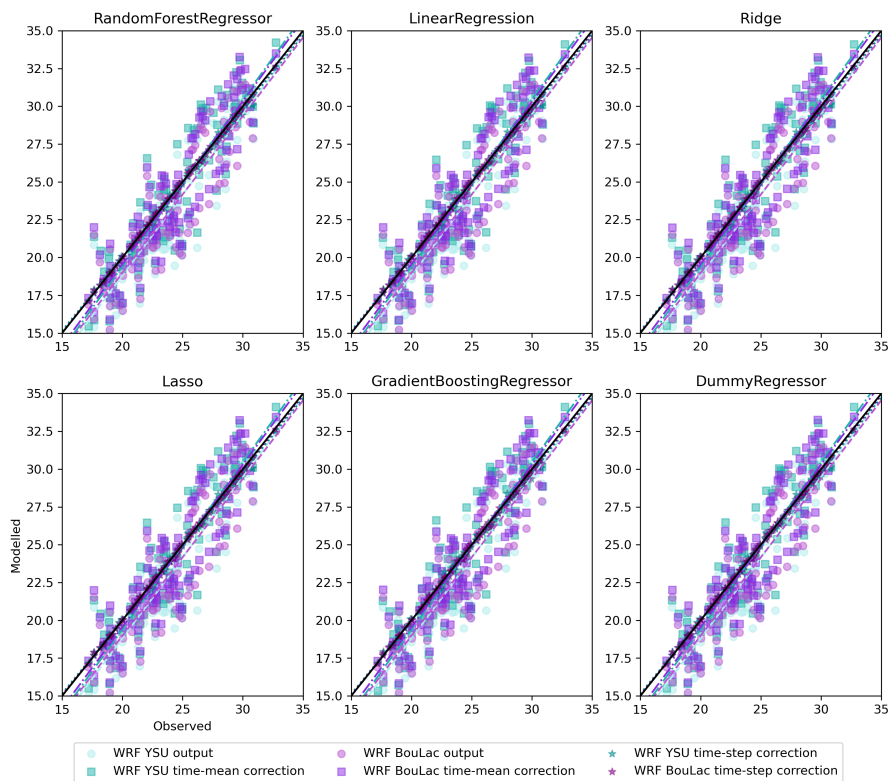


Figure B3. Same as figure B2, but for daily maximum temperatures.

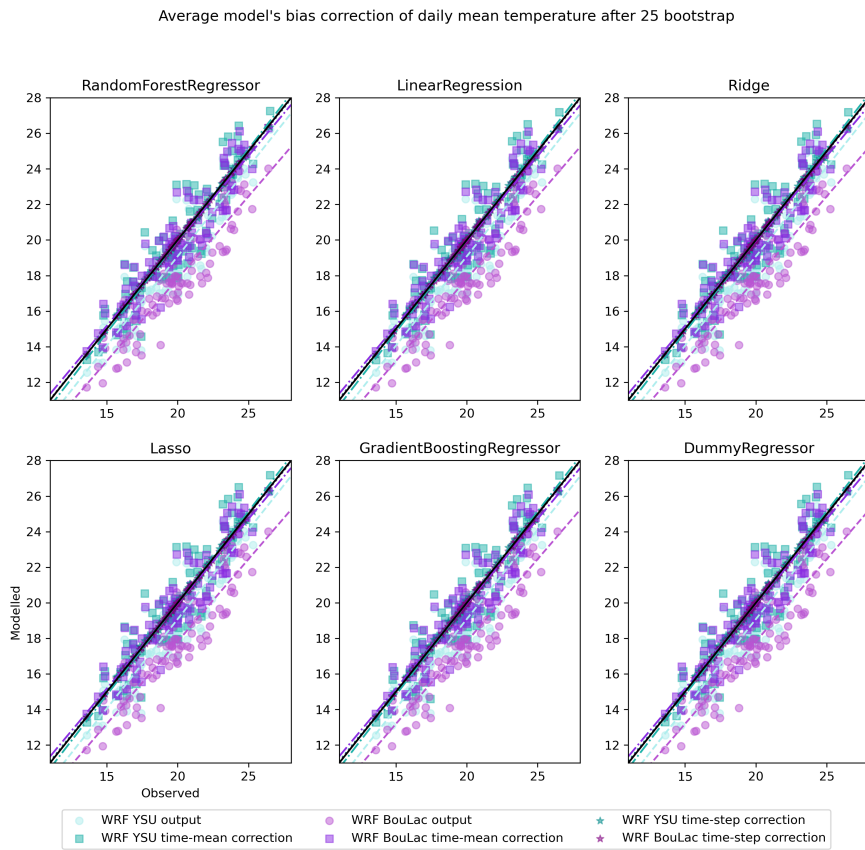


Figure B4. Same as figure B2, but for daily mean temperatures.

Modelled temperatures and respective bias-corrections with multiple regressors

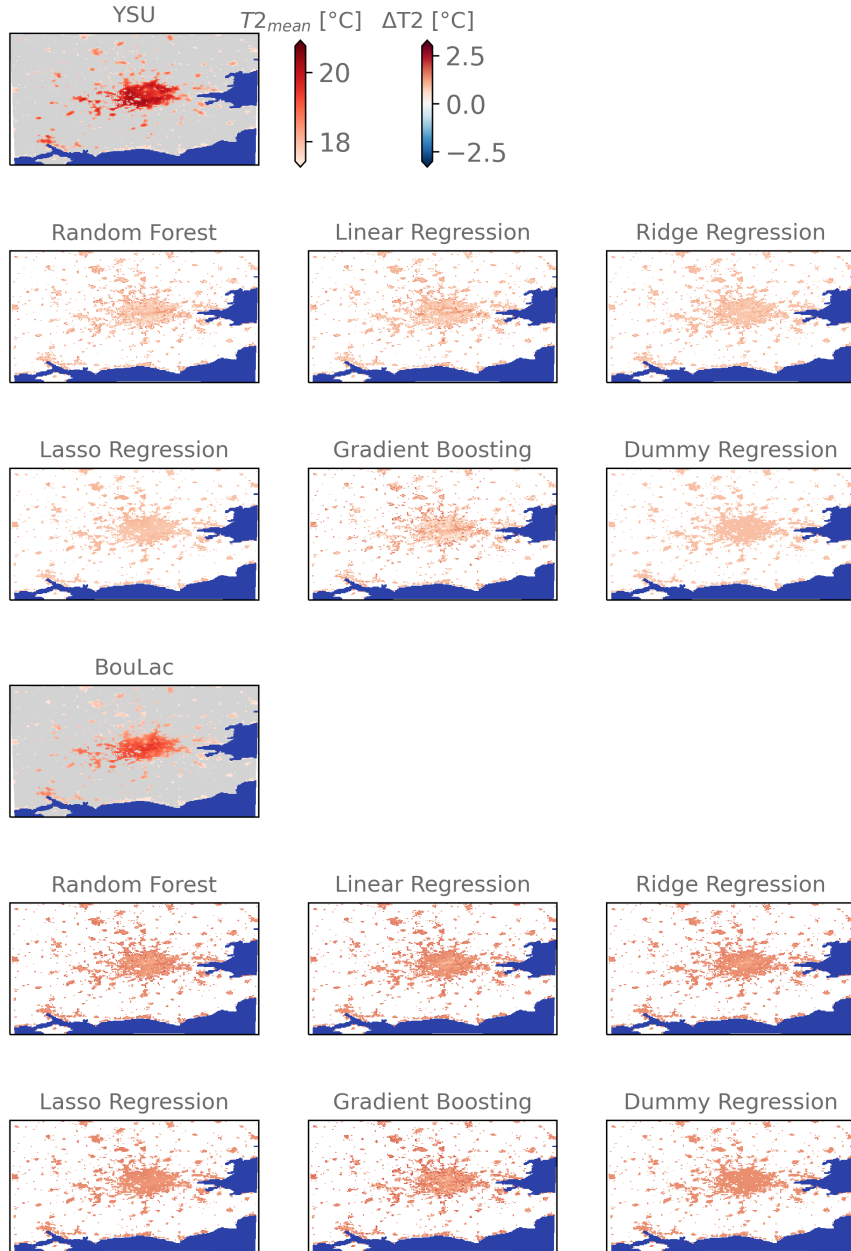


Figure B5. Same as figure 5, but for daily mean temperatures.

Modelled temperatures and respective bias-corrections with multiple regressors

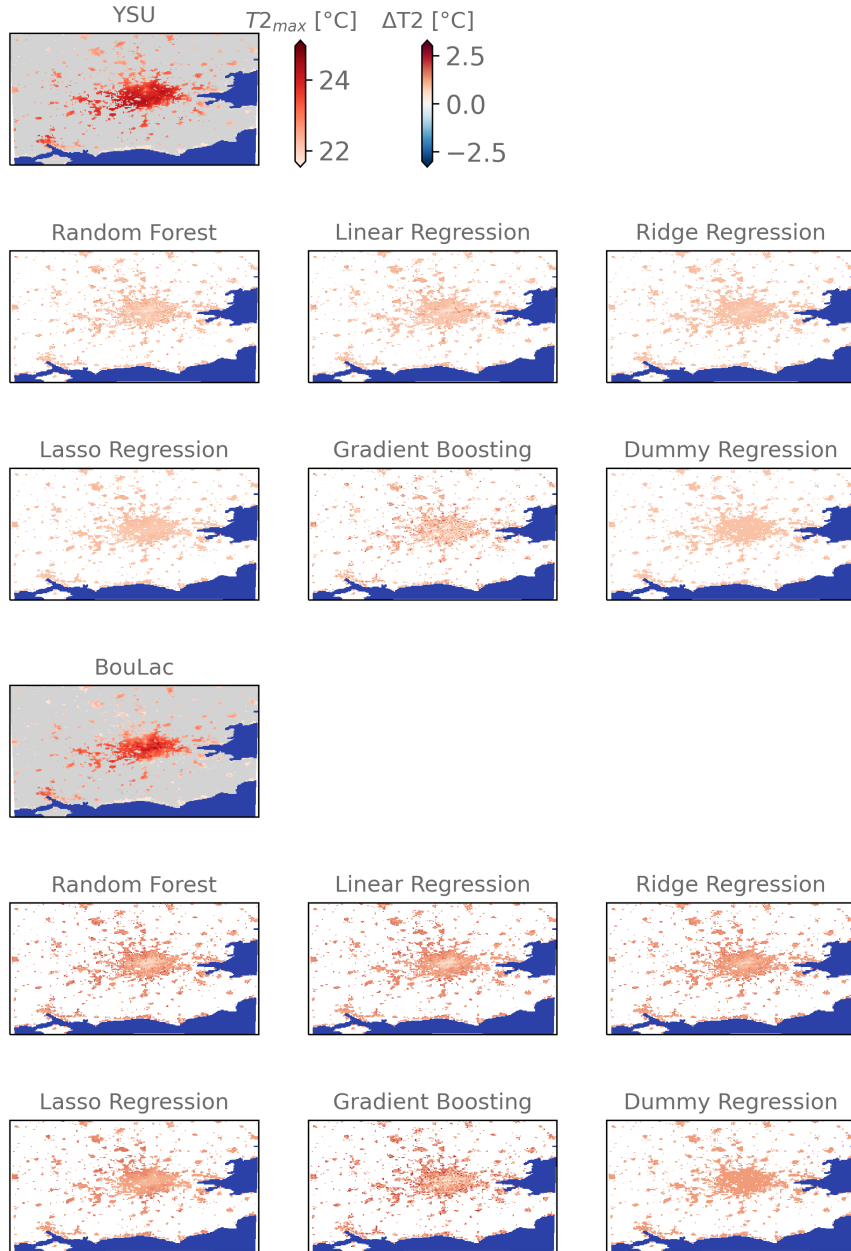


Figure B6. Same as figure 5, but for daily maximum temperatures.

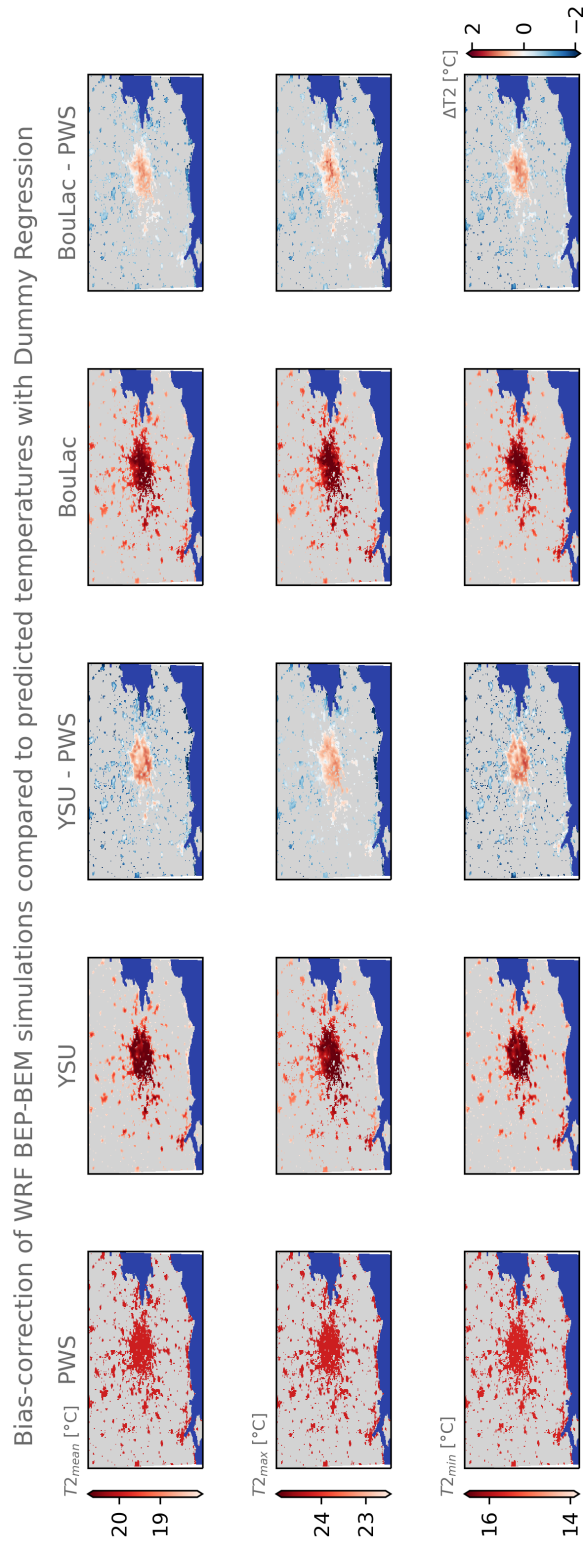


Figure B7. Same as figure 6, but for dummy regression.

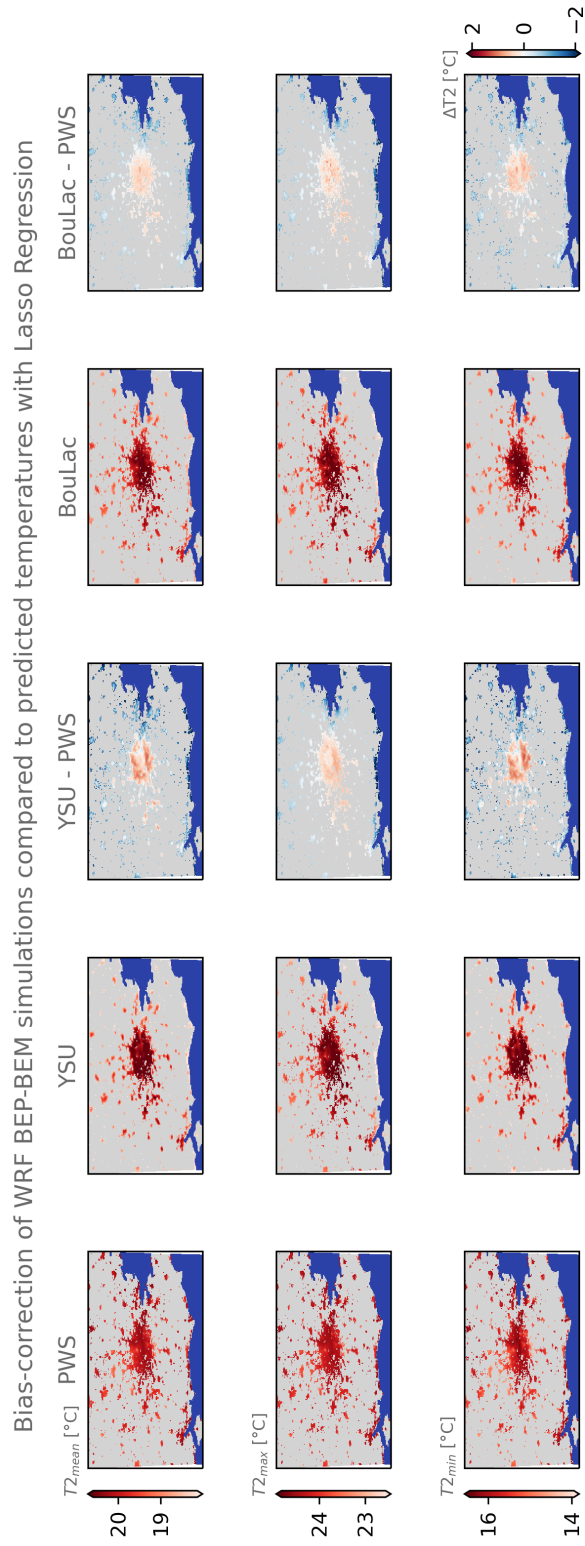


Figure B8. Same as figure 6, but for Lasso regression.

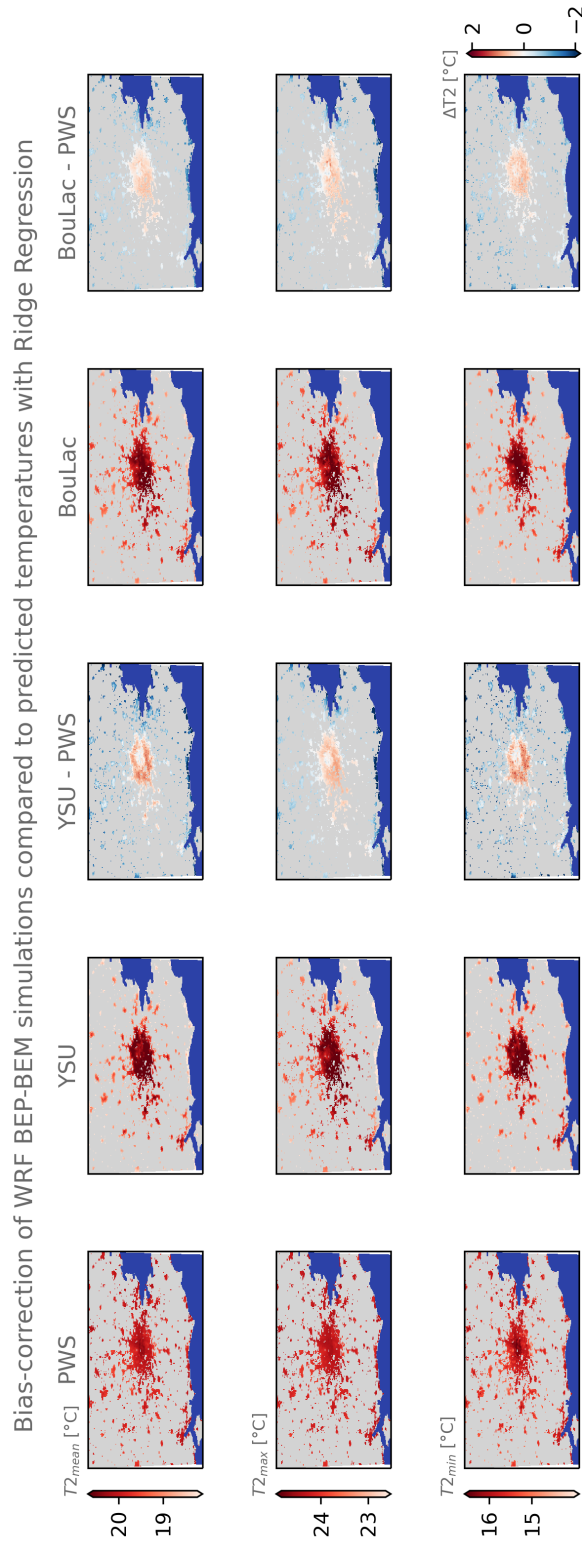


Figure B9. Same as figure 6, but for Ridge regression.

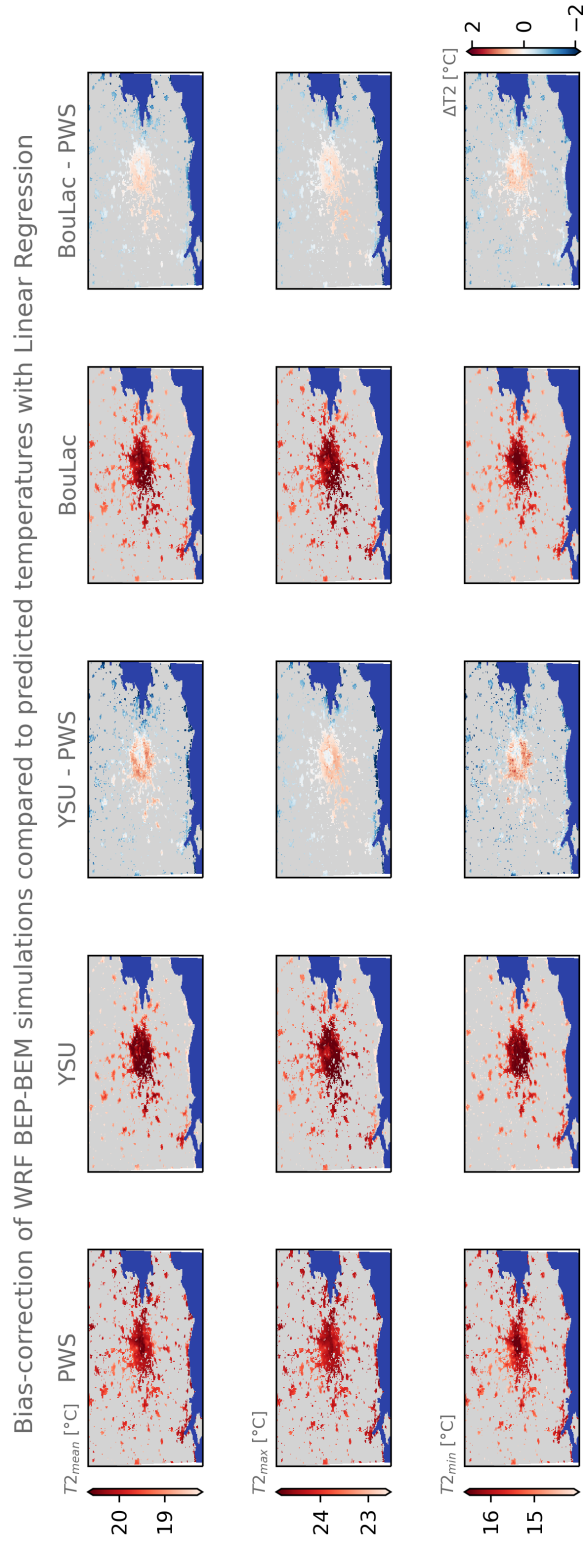


Figure B10. Same as figure 6, but for linear regression.

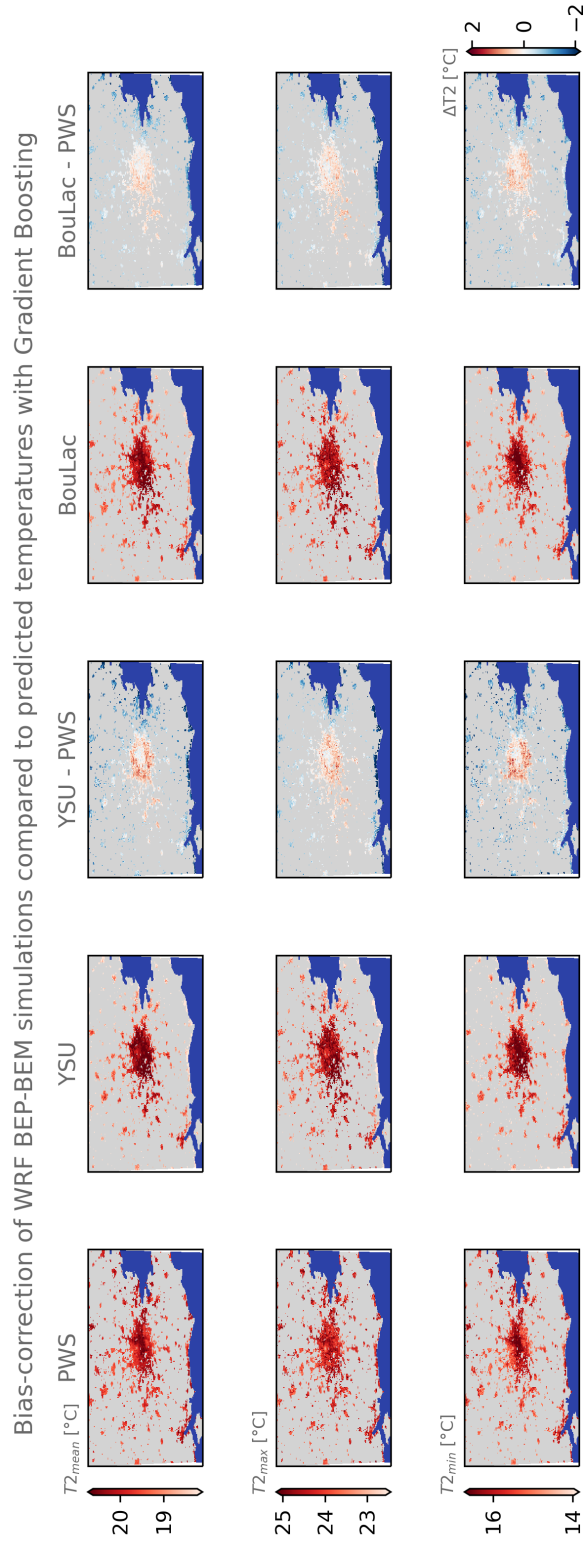


Figure B11. Same as figure 6, but for gradient boosting regression.